Journal of Medicinal Chemistry Article

J. Med. Chem. **2009,** *52,* 6685–6706 **6685**
DOI: 10.1021/jm9010127

Discovery of a Novel Class of Potent Coumarin Monoamine Oxidase B Inhibitors: Development and Biopharmacological Profiling of 7-[(3-Chlorobenzyl)oxy]-4-[(methylamino)methyl]-2*H*-chromen-2-one Methanesulfonate (NW-1772) as a Highly Potent, Selective, Reversible, and Orally Active Monoamine Oxidase B Inhibitor

Leonardo Pisani,[†,⊥] Giovanni Muncipinto,[†,⊥] Teresa Fabiola Miscioscia,[†] Orazio Nicolotti,[†] Francesco Leonetti,[†] Marco Catto,[†] Carla Caccia,[§] Patricia Salvati,[§] Ramon Soto-Otero,[‡] Estefania Mendez-Alvarez,[‡] Celine Passeleu,[∥] and Angelo Carotti*[,†]

[†]*Dipartimento Farmacochimico, Università degli Studi di Bari, Via Orabona 4, 70125-Bari, Italy,* [§]*Newron Pharmaceuticals Spa, Bresso (MI), Italy,* [‡]*Grupo de Neuroquímica, Departamento de Bioquímica y Biología Molecular, Facultad de Medicina, Universidad de Santiago de Compostela, Santiago de Compostela, Spain, and* [∥]*School of Pharmaceutical Sciences, University of Geneva, University of Lausanne, Switzerland.* [⊥] *L.P. and G.M. contributed equally to this work.*

Received July 9, 2009

In an effort to discover novel selective monoamine oxidase (MAO) B inhibitors with favorable physicochemical and pharmacokinetic profiles, 7-[(*m*-halogeno)benzyloxy]coumarins bearing properly selected polar substituents at position 4 were designed, synthesized, and evaluated as MAO inhibitors. Several compounds with MAO-B inhibitory activity in the nanomolar range and excellent MAO-B selectivity (selectivity index SI > 400) were identified. Structure−affinity relationships and docking simulations provided valuable insights into the enzyme−inhibitor binding interactions at position 4, which has been poorly explored. Furthermore, computational and experimental studies led to the identification and biopharmacological characterization of 7-[(3-chlorobenzyl)oxy]-4-[(methylamino)-methyl]-2*H*-chromen-2-one methanesulfonate **22b** (NW-1772) as an in vitro and in vivo potent and selective MAO-B inhibitor, with rapid blood−brain barrier penetration, short-acting and reversible inhibitory activity, slight inhibition of selected cytochrome P450s, and low in vitro toxicity. On the basis of this preliminary preclinical profile, inhibitor **22b** might be viewed as a promising clinical candidate for the treatment of neurodegenerative diseases.

Introduction

Monoamine oxidase (MAO,[a] EC 1.4.3.4, amine−oxygen oxidoreductase) is a membrane-bound flavoenzyme responsible for the oxidative deamination of xenobiotic amines[1] and monoamine neurotransmitters such as serotonin (5-HT), norepinephrine (NE), and dopamine (DA).[2] Two distinct enzymatic isoforms, named MAO-A and MAO-B, have been identified; they differ in amino acid sequence, three-dimensional structure, organ and tissue distribution, substrate specificity, and sensitivity to inhibitors.[3−9] Both enzymes oxidatively deaminate DA, whereas MAO-A preferentially deaminates 5-HT, epinephrine, and NE and is selectively inhibited by clorgyline. MAO-B preferentially metabolizes benzylamine and β-phenethylamine (PEA) and is selectively inhibited by selegiline and rasagiline (Chart 1).[10,11] The involvement of MAO in the metabolism of key neurotransmitters has made it an attractive target for pharmacological interventions in neurological disorders. The lack of selective inhibition, irreversible mechanism of action, severe side effects, e.g., hepatotoxicity and life-threatening hypertensive crisis, associated with the first-generation of antidepressant MAO-A inhibitors have stimulated further research aimed to the discovery of novel, less toxic drugs.[12,13] Several selective MAO-A inhibitors[14] acting as antidepressants (i.e., moclobemide,[15] brofaromine, clorgyline, and toloxatone; Chart 1), and selective MAO-B inhibitors acting as anti-Parkinson agents (i.e., lazabemide, selegiline, safinamide, and rasagiline; Chart 1)[16−18] have been discovered. Notably, rasagiline, approved by the U.S. Food and Drug Administration (FDA) as an anti-Parkinson drug, has been recently shown to be the first neuroprotective disease modifying drug for Parkinson's disease (PD).[19] In addition, selegiline has been recently approved as transdermal once-a-day patch formulation to treat major depressive disorders. The high doses of selegiline used in such a formulation may be responsible for MAO-A inhibition and, consequently, for the antidepressant effect.[20]

The MAO-B isoform is predominant in the human brain,[21] and its level increases significantly in aging-related neurodegenerative diseases (NDs).[22−24] As a consequence, neurotransmitters levels are lowered and oxidative stress[25−27] may be induced by highly reactive hydroxyl radicals formed in the reaction between hydrogen peroxide, produced during amine

*To whom correspondence should be addressed. Phone: +39-080-5442782. Fax: +39-080-5442230. E-mail: carotti@farmchim.uniba.it.

[a] Abbreviations: AD, Alzheimer's disease; FAD, flavin adenine dinucleotide; HDM, hexadecane membrane; MAO, monoamine oxidase; MAO-A, monoamine oxidase A; MAO-B, monoamine oxidase B; PAMPA, parallel artificial membrane permeability assay; PD, Parkinson's disease; PDB, Protein Data Bank; PLS-DA, partial least-squares discriminant analysis; PSA, polar surface area; SAFIR, structure−affinity relationships; SSR, structure−selectivity relationships.

Published on Web 10/07/2009

Chart 1. Chemical Structures of Nonselective and Selective MAO-A (A) and MAO-B (B) Inhibitors

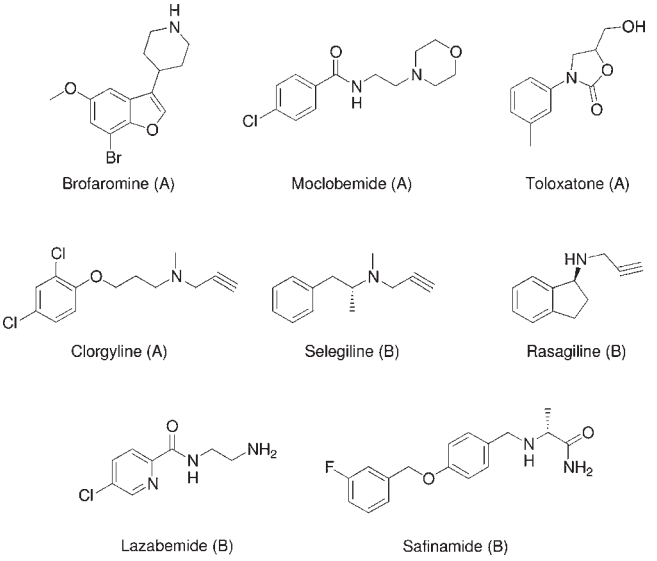

Scheme 1. Synthesis of 7-Hydroxycoumarin Intermediates **1a−d**[a]

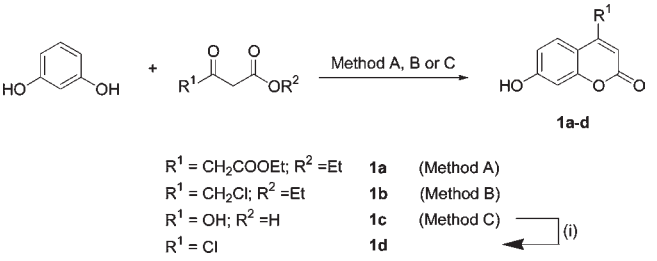

[a] Reagents and conditions: (method A) H_2SO_4 conc (cat.), 120 °C, 1 h; (method B) H_2SO_4 conc (large excess), 0 °C, 2 h; (method C) $BF_3 \cdot$diethyl etherate, 90 °C, 24 h; (i) $POCl_3$, reflux, 4 h.

Chart 2. Starting 4-Substituted-7-hydroxycoumarin Derivatives **1a,b,d,e** and **5**

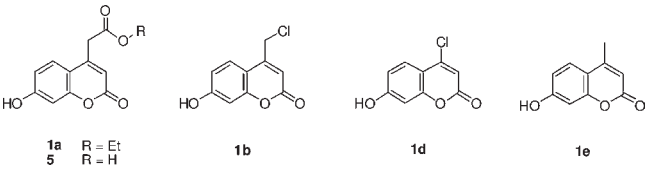

oxidation, and iron ion (Fenton's reaction).[28] Selective MAO-B inhibitors have therefore attracted new interest also as neuroprotective agents in the elderly and as potential drugs in the therapy of Alzheimer's disease (AD).[29,30] Indeed a pronounced neuroprotective effect of selegiline and rasagiline has been claimed[31,32] but clinical trials of selegiline in combination with antioxidants or acetylcholinesterase inhibitors and alone in AD have shown contrasting results.[33−35]

Although significant advances in the design of selective MAO inhibitors (MAOIs) have been achieved in the past 2 decades, a veritable breakthrough in the field occurred only a few years ago with the publication of the X-ray crystal structures of human MAO-B (hMAO-B)[5,36] and, to a lesser extent, rat MAO-A (rMAO-A).[8] The high-resolution 3D structure of hMAO-B[6] and, more recently, of hMAO-A[37] bound to selective, reversible, and irreversible inhibitors finally paved the way to the structure-based design of new and selective modulators of MAO activity. The wealth of information on structure and recently published methods for a medium throughput screening of MAOIs on cloned hMAOs[38,39] might be particularly helpful for a more efficient and faster discovery of new MAOIs.

As a part of our ongoing research in this field,[40−47] herein we report the design, synthesis, and biochemical evaluation of a new series of coumarins that maintained the potent and selective MAO-B inhibition found for this class of compounds[48−50] but that exhibited more appropriate physicochemical and pharmacokinetic properties for clinical applications as novel therapeutics of neurological disorders. In fact, most of the potent and selective MAO-B coumarin inhibitors studied so far have generally displayed too high lipophilicity and poor aqueous solubility, and this might strongly limit their investigations even at the level of experimental preclinical profiling. Guided by the wealth of information on structure−affinity and structure−selectivity relationships (SAFIRs and SSRs, respectively) developed for coumarinic MAO inhibitors,[45−47,51−53] we designed a series of novel MAO-B inhibitors, maintaining the benzyloxy and *m*-fluorobenzyloxy or *m*-chlorobenzyloxy substituents at position 7 and introducing adequate polar moieties, that is, cyano, amido, amidoamino, and aliphatic amino groups, at position 4. These limited, albeit crucial, structural modifications, if tolerated, would have enabled us to identify new MAO-B inhibitors with an improved pharmacokinetic profile and a higher druggability.

The results of this investigation, which led to the discovery of an in vitro and in vivo very potent, reversible, and selective MAO-B inhibitor exhibiting appropriate pharmacologic

Scheme 2. Synthesis of Compound **3** and Aminoacidic Coumarin Derivatives **4a−h** (Table 1)[a]

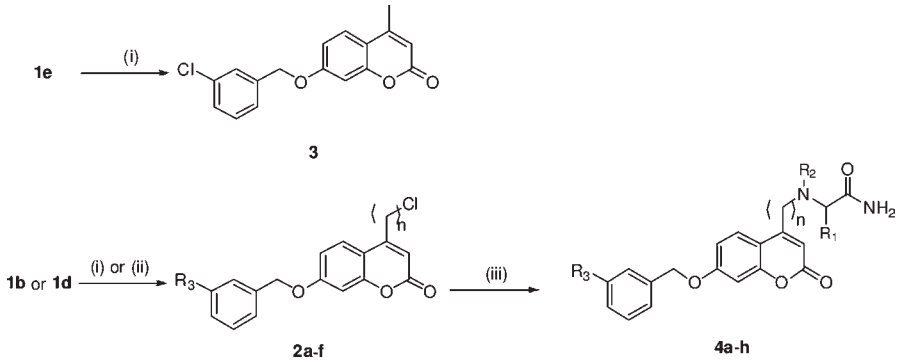

[a] Reagents and conditions: (i) $R_3C_6H_4CH_2Br$, K_2CO_3, EtOH, reflux, 2 h; (ii) piperonyl alcohol, DIAD, PPh_3, dry THF, room temperature, 18 h; (iii) $R_2NHCHR_1CONH_2 \cdot$HCl, DIEA, dry DMF, 80 °C, 5 h.

Scheme 3. Synthesis of Amidoaminocoumarin Derivatives **8a**−**c** (Table 2)[a]

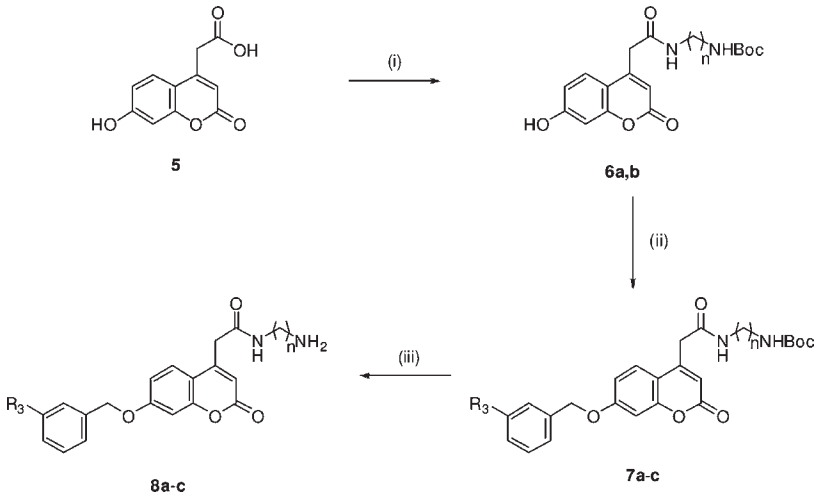

[a] Reagents and conditions: (i) $NH_2(CH_2)_nNHBoc$, DCC, HOBt, dry DMF, room temperature, 5 h; (ii) $R_3C_6H_4CH_2Br$, dry K_2CO_3, absolute EtOH, reflux, 0.5 h; (iii) TFA, CH_2Cl_2, room temperature, 20 min.

Scheme 4. Solid-Phase Synthesis of Primary Amides **11a**−**d** and **13a**,**b** (Table 2)[a]

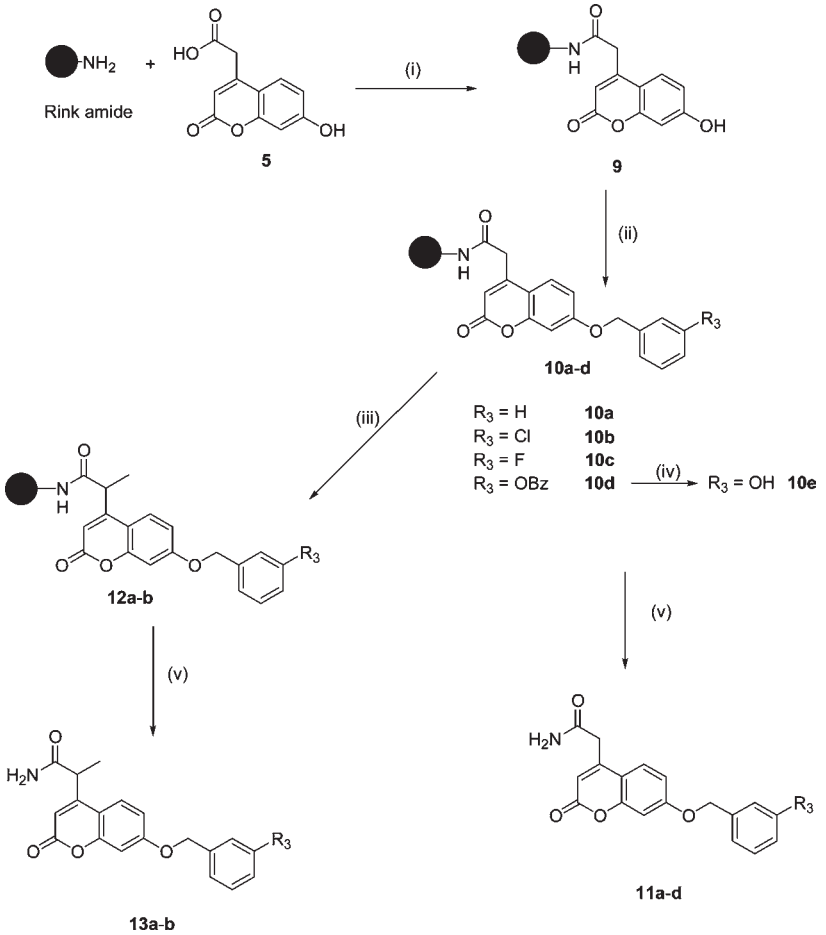

[a] Reagents and conditions: (i) DIC, HOBt, dry DMF, room temperature, 15 h; (ii) DIEA, $R_3C_6H_4CH_2Br$ or **17**, dry DMF, 70 °C, 2.5 h; (iii) KHMDS, CH_3I, dry DMF, room temperature, 4 h; (iv) CH_3ONa, dry THF, room temperature, 4 h; (v) TFA/H_2O/TES, 9.5/0.25/0.25, room temperature, 1 h.

features to be progressed to clinical trials, will be presented and discussed in this paper, along with new SAFIRs, SSRs, and docking studies that provided a consistent picture of the main binding interactions modulating the MAO inhibitory potency and MAO-B isoform selectivity of this new class of coumarins. The data discussed in the present paper have been anticipated in part in a patent[48] and at the ACS-EFMC meeting of medicinal chemistry.[54]

Chemistry

The synthesis of the novel coumarin derivatives was performed according to the reaction pathways illustrated in

Schemes 1−10. The starting 7-hydroxycoumarin intermediates **1a**,**b**,**d**,**e** and **5** depicted in Chart 2 were obtained through the well-known von Pechmann reaction[55] with slight modifications[56,57] depending on the stability and reactivity of the β-dicarbonyl reagent used (Scheme 1).

Chlorination of derivative **1c** in refluxing phosphorus oxychloride yielded regioselectively coumarin **1d**. The benzylation of **1b**,**d**,**e** with the appropriate benzyl bromide furnished target compound **3** and intermediate chlorides **2a**−**e** (Scheme 2).

Intermediate piperonyl chloride **2f** was prepared through a Mitsunobu reaction[58] starting from 7-hydroxycoumarin **1b** and piperonyl alcohol in the presence of diisopropyl azodicarboxylate (DIAD) and triphenylphospine (PPh_3). Chlorides **2a**−**f** were reacted with suitable, commercially available (*S*)-α-aminoamides, affording the target coumarins **4a**−**h** (Scheme 2).

DCC-HOBt mediated coupling of commercially available acid **5** and mono-Boc-protected hydrazine or ethylenediamine represented the first step for the synthesis of compounds **8a**−**c** (Scheme 3). The resulting amides **6a**,**b** were benzylated at the 7-OH and then reacted with TFA in CH_2Cl_2 to remove the Boc protecting group. The selective benzylation of the 7-OH was problematic because of competitive alkylations at the acidic methylenic group at position 4 and at the amidic nitrogen of low sterically hindered secondary amides. The elimination of these undesired side reactions was accomplished by applying a solid-phase protocol to prepare primary amides **11a**−**d** and the corresponding C-methylated analogues **13a**,**b** (Scheme 4). 7-Hydroxycoumarinacetic acid **5** was loaded onto a Rink amide, followed by a benzylation reaction that proceeded cleanly, without the formation of byproduct, yielding the derivatized resins **10a**−**c**. Regioselective methylation of the 4-CH_2 group was obtained using a strong and bulky base (potassium hexamethyldisilazane, KHMDS) and methyl iodide to afford resins **12a**,**b**. The target amides **11a**−**d** and

Scheme 5. Synthesis of Benzoate **17**[a]

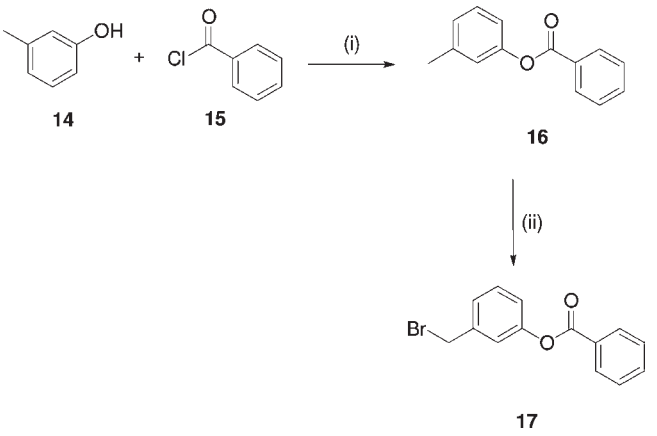

[a] Reagents and conditions: (i) TEA, dry THF, room temperature, 0.5 h; (ii) NBS, AIBN, CCl_4, reflux, 1 h.

Scheme 6. Synthesis of 7-Pyridylmethoxycoumarin Derivatives **19a**,**b** (Table 2)[a]

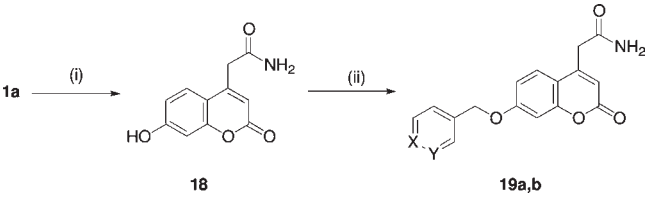

[a] Reagents and conditions: (i) aq NH_3, sealed tube, 90 °C, 60 h; (ii) 3- or 4-pyridinylmethanol, PBu_3, ADDP, dry THF, room temperature, 18 h.

Scheme 7. Synthesis of Amidocoumarin Derivatives **21a**−**g** (Table 2)[a]

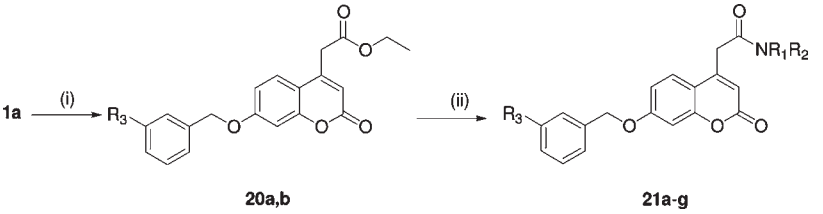

[a] Reagents and conditions: (i) ADDP, PPh_3, $R_3C_6H_4CH_2OH$, dry THF, room temperature, 18 h; (ii) R_1R_2NH, dry THF, 90 °C, sealed tube, 24−60 h.

Scheme 8. Synthesis of Aminocoumarin Derivatives **22a**−**k** and **24a**,**b** (Table 3)[a]

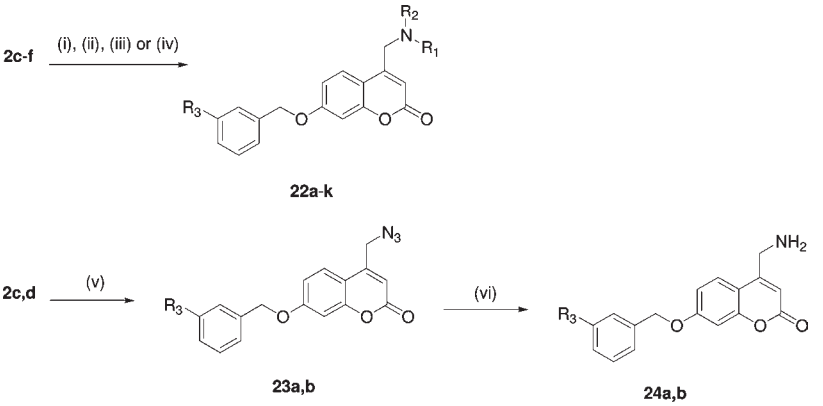

[a] Reagents and conditions: (i) R_1R_2NH, dry THF, 50 °C, 5 h; (ii) $EtNH_2$ 70% water solution, room temperature, 3 h; (iii) isopropylamine, reflux, 2 h; (iv) *N*-methylbenzylamine or benzylamine, K_2CO_3, EtOH, reflux, 2−5 h; (v) sodium azide, EtOH, reflux, 2 h; (vi) $SnCl_2$, MeOH, room temperature, 3 h.

Scheme 9. Synthesis of 4-Aminoethylcoumarin Derivative **26** (Table 3)[a]

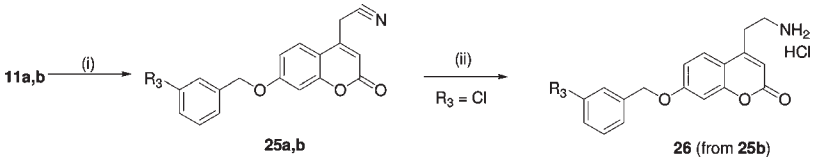

[a] Reagents and conditions: (i) TFAA, dry pyridine and dioxane, 0 °C to room temperature, 10 min; (ii) $NaBH_4/CoCl_2$, MeOH, room temperature, 1 h.

Scheme 10. Synthesis of 4-Aminoethylcoumarin Derivatives **30a**,**b** (Table 3)[a]

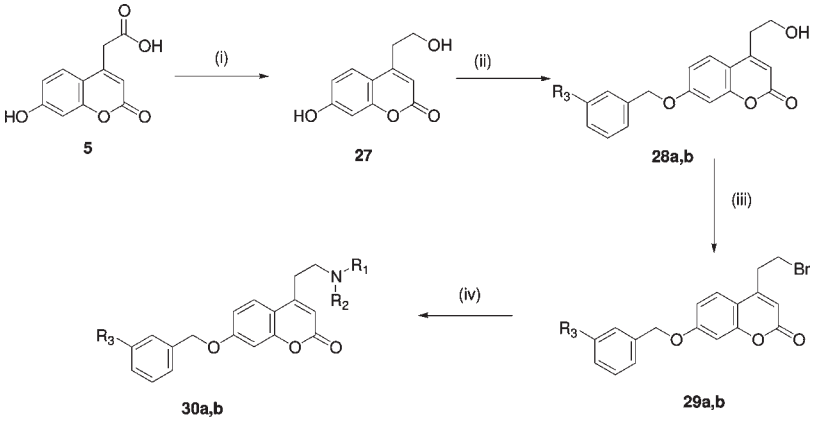

[a] Reagents and conditions: (i) $BH_3 \cdot$THF complex, dry THF, room temperature, 6 h; (ii) $R_3C_6H_4CH_2Br$, K_2CO_3, EtOH, reflux, 45 min; (iii) CBr_4, PPh_3, dry CH_2Cl_2, room temperature, 1 h; (iv) R_1R_2NH, K_2CO_3, KI, dry THF, 50 °C, 15 h.

13a,**b** were obtained upon cleavage from the resin with a TFA/H_2O mixture containing triethylsilane as proton scavenger.

The preparation of amide **11d** required different additional synthetic steps consisting of the removal of the benzoyl protecting group with sodium methoxide (from resin **10d**) and of the separated synthesis of benzyl bromide **17** (Scheme 5) that began with the benzoylation of *m*-cresol followed by the bromination of ester **16** with NBS and AIBN.

The ammonolysis of ester **1a** with aqueous NH_3 in a sealed tube afforded amide **18** in excellent yields. The introduction of 3- and 4-pyridinylmethoxy moiety at position 7 (compounds **19a**,**b**; Scheme 6) was performed following a standard Mitsunobu protocol with tributylphosphine (PBu_3) and 1,1′-(azodicarbonyl)dipiperidine (ADDP), thus avoiding the use of relatively unstable pyridylmethyl bromides.

As described in Scheme 7, preliminary benzylation reaction of 7-hydroxycoumarin **1a** under Mitsunobu conditions afforded the esters **20a**,**b** that were reacted with a suitable aliphatic amine to yield secondary and tertiary amides **21a**−**g**.

As outlined in Scheme 8, the substituted amines **22a**−**k** were easily obtained by nucleophilic substitution of chlorides **2c**−**f** with the appropriate amines. Primary amines **24a**,**b** were synthesized from azides **23a**,**b** obtained by refluxing chlorides **2c**,**d** with sodium azide in ethanol, as illustrated in Scheme 8. In this case, despite the tedious and potentially toxic purification procedure, $SnCl_2$ proved to be the most effective method for reducing azides compared to the traditional Staudinger reduction with PPh_3/H_2O,[59] Sn(II)/thiophenol/triethylamine[60] reducing system, or catalytic hydrogenation.

The elongation of the aliphatic bridge linking the aminic moiety at position 4 to the coumarin ring was pursued according to the reaction pathway illustrated in Scheme 9. Amides **11a**,**b** were converted into the corresponding nitriles **25a**,**b** upon treatment with trifluoroacetic anhydride in pyridine according to an efficient method developed by some of us many years ago.[61] The reduction of nitrile **25b** with sodium borohydride and $CoCl_2$ afforded the desired primary amine **26**. An alternative synthetic pathway (Scheme 10) was followed to access secondary and tertiary amines.

The carboxylic group of compound **5** was selectively reduced by the BH_3−THF complex, and the resulting dihydroxylated derivative **27** was benzylated at the phenolic OH in the presence of potassium carbonate and a catalytic amount of KI in refluxing ethanol. The alcohols **28a**,**b** underwent an Appel-type mild bromination with CBr_4 and PPh_3. The subsequent nucleophilic displacement of the bromide anion with the appropriate amine yielded the final amines **30a**,**b**.

Physicochemical Assays

log *P*, pK_a, and Aqueous Solubility Measurements. The pK_a and octanol−water partition coefficient were measured by potentiometric methods[62] with a Sirius GLpKa instrument. Aqueous solubility was determined with the DMSO−buffer dilution turbidimetric method[63] according to a reported procedure.[64]

PAMPA Permeation Assay. Selected MAO inhibitors were analyzed using PAMPA (parallel artificial membrane permeability assay), a method recently developed for the rapid determination of passive transport.[65] In PAMPA, an artificial liquid membrane is used to separate two compartments, one containing a buffer solution of compounds to be tested (defined as the donor compartment) and the other an initial fresh buffer solution (defined as the acceptor compartment) assembled in a "sandwich-like" configuration. The permeation of tested compounds through the artificial membrane is determined after a fixed incubation time by disassembling the "sandwich" and measuring sample concentrations in the donor and acceptor compartments.

Chart 3. General Structures of Novel 4,7-Disubstituted Coumarin MAOIs (Tables 1−4)

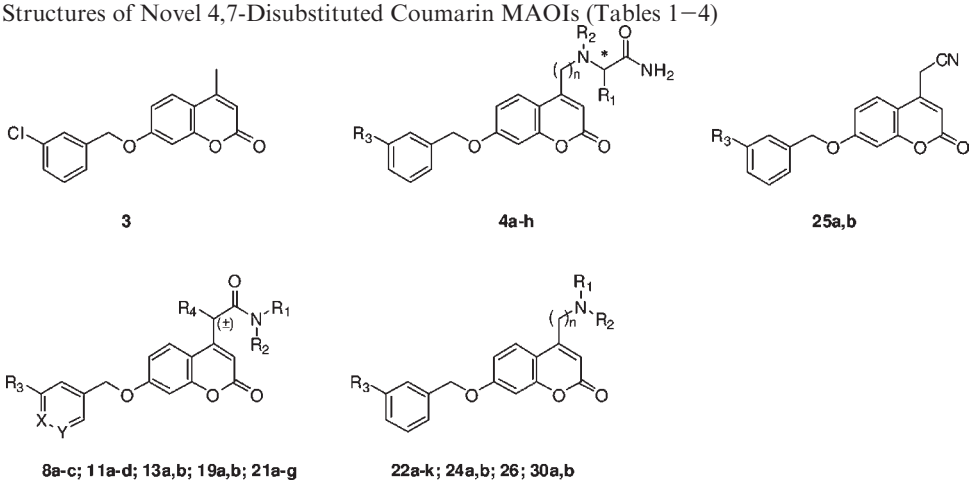

Table 1. MAO Inhibitory Activity of (*S*)-Aminoamidocoumarin Derivatives **4a**−**h**

compd	*n*	R_1	R_2	R_3	MAO-A[a]	MAO-B[a]	SI[b]
4a	0	CH_3	H	H	100	0.68	147
4b	0	CH_3	H	Cl	35%	0.21	
4c	0	$-CH_2CH_2CH_2-$		H	99.8	16.1	6
4d	0	$-CH_2CH_2CH_2-$		Cl	5%	9.60	
4e	0	CH_2OH	H	Cl	>100	2.40	>42
4f	1	CH_3	H	H	22.7	1.80	13
4g	1	$-CH_2CH_2CH_2-$		H	35	0.38	92
4h	1	$-CH_2CH_2CH_2-$		F	>100	0.85	>117

[a] IC_{50} (μM) or % inhibition at 10 μM. [b] SI = [IC_{50} MAO-A (μM)]/[IC_{50} MAO-B (μM)].

The HDM-PAMPA (hexadecane membrane assay targeting GI track) assay developed by Wohnsland and Faller,[65] making use of an artificial liquid membrane composed of hexadecane supported on polycarbonate filters for the prediction of passive transcellular permeability, was used as a low cost and efficient alternative to the Caco-2 cell culture model.[66]

Biological Assays

In Vitro MAO Inhibition. Rat brain mitochondria were used as the source for the two MAO isoforms. MAO enzymatic activities were assessed with a radioenzymatic assay using ^{14}C-serotonin (5-HT) and ^{14}C-phenylethylamine (PEA) as selective radiosubstrates for MAO-A and MAO-B, respectively, according to a well consolidated procedure.[67] For compound **22b** the MAO-B radioenzymatic assay was performed also in human platelet rich plasma (PRP).[68]

In Vitro MAO B Reversibility Inhibition Studies. The reversible nature of MAO-B inhibition was assessed by evaluating the enzymatic activity upon different incubation time experiments. Time-dependent association kinetics were measured as the IC_{50} values after 0 and 30 min enzyme−inhibitor incubation in the assay medium.

Ex Vivo MAO Inhibition. Mice were treated with the test compound at different oral and intraperitoneal concentrations and sacrificed at different time intervals. The brains were removed, and crude homogenates were prepared in 0.1 M phosphate buffer, pH 7.40. Ex vivo MAO-A and MAO-B enzymatic activities were assessed according to the radioenzymatic assay described above.

In Vitro Human Recombinant Cytocrome P450 Isoform Assay. Inhibition of six key cytochrome P450 isoforms (CYP1A2, CYP2C9, CYP2C19, CYP2D6, CYP2E1, and CYP3A4) was measured in distinct assays by using specific substrates that become fluorescent upon CYP-promoted metabolism (Gentest Kit assay, BD Biosciences, Bedford, MA).

In Vitro Cell Viability Assay. The SHSY-5Y continuous cell line from a human neuroblastoma was used and cell viability measured by the colorimetric MTS assay.[69]

Computational and Molecular Modeling Studies

Building and optimization of small molecules and MAO homology modeling were performed with Sybyl (Tripos, St. Louis, MO) and Modeller (DBSPC, University of California—San Francisco, San Francisco, CA) software, respectively. Docking simulations were carried using the GOLD program (Cambridge Crystallographic Data Centre, Cambridge, U.K.).

Polar surface area (PSA), a molecular descriptor largely used to roughly estimate oral bioavailability of potential drugs,[70] and LogBBB, a parameter related to the drug capability to cross the blood brain barrier (BBB)[71] were calculated by using Volsurf+ (Molecular Discovery, Perugia, Italy).

Results and Discussion

4-Methyl-7-(*m*-chlorobenzyloxy)coumarin **3** was designed and synthesized as the compound bearing the simplest hydrophobic substituent at position 4. It was considered as an appropriate reference compound to which the biochemical, physicochemical, and pharmacokinetic properties of the newly designed 4,7-disubstituted coumarins, bearing polar groups at position 4, were to be compared.

Compound **3** exhibited high in vitro MAO-B affinity and a very low affinity to MAO-A (IC_{50} of 0.007 and 5.2 μM, respectively). Its estimated lipophilicity and aqueous solubility indicated a high octanol−water partition coefficient (P; log P = 4.73, from Bioloom-BioByte Corp., Claremont, CA) and a poor aqueous solubility ($S = 2.63 \times 10^{-5}$ M, from ACD, version 12, Advanced Chemistry Development, Toronto, Canada).

The chemical structures of the newly designed series of 4,7-disubstituted coumarins are shown in Chart 3, whereas their MAO-A and MAO-B affinities and selectivity indices are listed in Tables 1−4.

Inhibition data of both MAO isoforms are reported as IC_{50} (μM) or as the percentage of inhibition at the indicated concentration for low-active inhibitors. Selectivity was expressed as selectivity index (SI), which is the ratio of the IC_{50} of MAO-A to the IC_{50} of MAO-B. For an immediate and more efficient analysis of SAFIRs and SSRs, inhibition data

Table 2. MAO Inhibitory Activity of Amidocoumarin Derivatives **8a**−**c**, **11a**−**d**, **13a**,**b**, **19a**,**b**, and **21a**−**g**

compd	R_1	R_2	R_4	R_3	X	Y	MAO-A[a]	MAO-B[a]	SI[b]
8a	H	NH_2	H	H	CH	CH	1.44	0.040	36
8b	H	NH_2	H	Cl	CH	CH	2.50	0.090	28
8c	H	$(CH_2)_2NH_2$	H	Cl	CH	CH	>100	>10	nd
11a	H	H	H	H	CH	CH	8.0	0.20	40
11b	H	H	H	Cl	CH	CH	26	0.030	867
11c	H	H	H	F	CH	CH	70	0.050	1400
11d	H	H	H	OH	CH	CH	4.27	1.0	4
19a	H	H	H	H	CH	N	21.0	1.30	16
19b	H	H	H	H	N	CH	26.5	2.0	13
21a	Me	H	H	H	CH	CH	2.80	0.015	187
21b	Me	H	H	Cl	CH	CH	0.50	0.024	21
21c	Bu	H	H	Cl	CH	CH	>100	>10	nd
21d	Bn	H	H	Cl	CH	CH	>100	5.0	>20
21e	Me	Me	H	H	CH	CH	23.1	0.40	58
21f	Me	Me	H	Cl	CH	CH	>100	0.040	>2400
21g	Bu	Me	H	Cl	CH	CH	>100	>10	nd
13a[c]	H	H	Me	H	CH	CH	6.26	0.10	63
13b[c]	H	H	Me	F	CH	CH	2.0	0.10	20

[a] IC_{50} (μM). [b] SI = [IC_{50} MAO-A (μM)]/[IC_{50} MAO-B (μM)]. [c] Tested as racemate.

Table 3. MAO Inhibitory Activity of Aminocoumarin Derivatives **22a**−**k**, **24a**,**b**, **26**, and **30a**,**b**

compd	*n*	R_1	R_2	R_3	MAO-A[a]	MAO-B[a]	SI[b]
22a	1	CH_3	H	H	15.4	0.028	550
22b[c]	1	CH_3	H	Cl	5.94	0.013	457
22c[c]	1	CH_3	H	F	13.5	0.018	750
22d	1	CH_3	H	*e*	5.40	0.020	270
22e[c]	1	CH_2CH_3	H	F	22.6	0.10	226
22f[c]	1	$CH(CH_3)_2$	H	F	91.0	3.80	24
22g	1	Bn	H	Cl	>100	3.60	>28
22h	1	CH_3	CH_3	H	100	1.80	56
22i	1	CH_3	CH_3	Cl	50.8	1.12	45
22j	1	CH_3	CH_3	F	>100	0.51	>196
22k	1	CH_3	Bn	Cl	>100	8.0	>13
24a	1	H	H	H	4.40	0.021	210
24b	1	H	H	Cl	2.0	0.015	133
26[d]	2	H	H	Cl	31.8	0.25	127
30a	2	CH_3	H	Cl	74.0	0.30	247
30b	2	CH_3	CH_3	H	25.9	0.46	56

[a] IC_{50} (μM). [b] SI = [IC_{50} MAO-A (μM)]/[IC_{50} MAO-B (μM)]. [c] Tested as mesylate. [d] Tested as hydrochloride. [e] $R_{meta-para}$ = $-OCH_2O-$.

Table 4. MAO Inhibitory Activity of 4-Cyanomethylcoumarin Derivatives **25a**,**b**

compd	R_3	MAO-A[a]	MAO-B[a]	SI[b]
25a	H	0.20	0.23	0.9
25b	Cl	0.47	0.016	29

[a] IC_{50} (μM). [b] SI = [IC_{50} MAO-A (μM)]/[IC_{50} MAO-B (μM)].

are presented also in Figure 1 as a plot of pIC_{50} of MAO-B (*x*-axis) versus pIC_{50} of MAO-A (*y*-axis) using the same scale and range for both axes (square plot). For immediate location, the different classes of coumarin inhibitors, i.e., aminoamides (Table 1), carboxyhydrazides and amides (Table 2), amines (Table 3), nitriles (Table 4), and the reference compound **3** are indicated in the plot with differently colored circles. Unfortunately, the low MAO-A affinity, often associated with a limited solubility in the aqueous assay medium, did not permit the measurement of IC_{50} (IC_{50} > 100 μM) for some compounds, and therefore, they are not shown in the plot. To avoid the loss of an important data point, compound **21f**, which is a potent and selective MAO-B inhibitor, was plotted with an estimated pIC_{50} of MAO-A equal to 3.50.

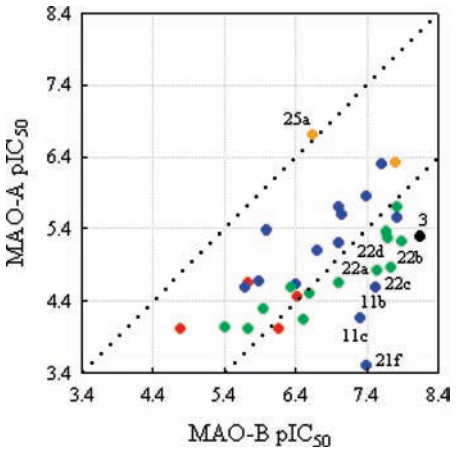

Figure 1. Square plot of rMAO affinity and selectivity. The different classes of coumarin inhibitors in Tables 1−4 and reference compound **3** are indicated with red, blue, green, orange, and black circles, respectively. Bottom-right corner contains potent and highly selective rMAO-B inhibitors. The most potent and selective MAO-B inhibitors are highlighted by black labels along with the only nonselective inhibitor **25a**.

Compounds with identical affinities at both isoenzymes lie on the bisector ($y = x$) of the graph, whereas highly selective MAO-B inhibitors lie well below the bisector, the distance of their pIC_{50} values from the bisector being a direct measure of their degree of selectivity. A line traced at two pIC_{50} unit distance below the bisector enables the straightforward location of inhibitors with a selectivity index−affinity ratio (SI) higher than 100 (i.e., $\Delta pIC_{50} > 2$).

At a first glance, the plot indicates that very potent and selective MAO-B inhibitors were discovered and that no apparent relationship exists between MAO-A and MAO-B inhibitory affinities. Only the cyano derivative **25a** lies on the bisector, exhibiting nearly equal affinity to both enzymes. MAO-A affinity was generally very low, and only in a very few cases, i.e., for the two cyanomethyl derivatives **25a**,**b** and the *N*-methylcarboxamidomethyl derivative **21b**, did affinities reach the submicromolar range.

Inhibitors endowed with both high MAO-B affinity and selectivity (i.e., both high pIC_{50} and SI values) are located at the bottom of the right-hand corner of the plot and belong mostly to the aminic and the amidic series (Tables 2 and 3, respectively). The most interesting compounds in terms of MAO-B affinity and selectivity, e.g., amides **22a**−**d** and amines **11b**,**c**, are highlighted in the plot.

A comparison of the MAO-B inhibition of 4-CH_2X-7-(*m*-chlorobenzyloxy)coumarins (Tables 1−4) revealed the following order of potency **24b** ≥ **25b** > **11b** > **8b** > **4b** > **26**, suggesting that the simple cyano, primary amino, and amido groups (X = CN, NH_2, and $CONH_2$, respectively) are highly preferred polar substituents at position 4 for an efficient binding to MAO-B.

A similar comparison of the MAO-B affinity of differently meta-substituted benzyloxy derivatives revealed that inhibitors bearing *m*-chloro and -fluoro substituents were generally more active than the corresponding benzyl-unsubstituted parent compounds. Moreover, the replacement of the 7-benzyloxy group with the 3- and 4-pyridylmethoxy isosteric substituents led to a significant decrease of affinity (compare **11a** vs **19a** and **19b**). These results are in full agreement with our previous

findings and confirm that the lipophilicity of the substituent at position 7 plays a crucial role in selective and efficient binding to MAO-B.[45,46,72]

The most salient results emerging from a careful evaluation of the MAO-B affinity and selectivity variation within the different classes of coumarin derivatives reported in Tables 1−3 can be summarized as follows.

A dramatic reduction of MAO-B affinity, in comparison with reference compound **3**, was observed for all the synthesized alanyl-, prolin-, and serin-amide derivatives **4** (Table 1) bearing the α-aminoamido moiety directly linked to the coumarin ring (i.e., **4a**−**e**) or bridged to it through a methylenic unit (i.e., **4f**−**h**). The less active MAO-B inhibitors were the more rigid prolinamide derivatives **4c**,**d**, whereas alaninamide derivatives **4a**,**b** and the more conformationally flexible prolinamide derivatives **4g**,**h** exhibited submicromolar MAO-B affinities. The SIs ranged from 6 to 147, and no clear SSR emerged from their analysis.

Nanomolar MAO-B inhibitory potencies were shown by 4-carboxyhydrazidomethylcoumarin derivatives **8a**,**b** and by the 4-carboxamidomethylcoumarin, 4-*N*-methylcarboxamidomethylcoumarin, and 4-*N*,*N*-dimethylcarboxamidomethylcoumarin derivatives **11b**,**c**, **21a**,**b**, and **21f**, respectively. MAO-B affinity of 7-*m*-chlorobenzyloxy derivatives remained high and nearly constant going from carboxamido (**11b**) to *N*-methylcarboxamido (**21b**) and to *N*,*N*-dimethylcarboxamido (**21f**) coumarin derivatives but dramatically diminished as the size of the *N*-alkyl substituent(s) increased as in compounds **21c**,**d**,**g**. As previously anticipated, the isosteric substitution of the 7-benzyloxy group with the 3- and 4-pyridylmethoxy groups led to a significant decrease of affinity (compare **19a**,**b** vs **11a**). C-Methylated 7-*m*-chlorobenzyloxy and 7-*m*-fluorobenzyloxy racemates **13a**,**b** displayed high and equal affinities to MAO-B. Compound **8c**, an *N*-aminoethyl derivative of the 4-carboxamidomethylcoumarin **11b**, was found completely inactive at both MAO isoforms. Potent and highly selective MAO-B inhibitors were found in the class of 4-carboxamidomethylcoumarins in Table 2. The 7-*m*-halogenobenzyloxy derivatives **11b**,**c** and **21f** exhibited IC_{50}/SI values equal to 0.030/867, 0.050/1400, and 0.040/2400, respectively. Very surprisingly, the *N*-methylcarboxamide **21b** was endowed with the highest MAO-A affinity of the entire series of tested inhibitors. Conversely, its close *N*,*N*-dimethyl analogue **21f** was completely inactive at the same enzyme isoform ($IC_{50} > 100\ \mu M$). This striking difference was quite unexpected and very difficult to interpret.

Affinity data of 4-aminomethyl- and 4-aminoethylcoumarins (Table 3) indicated that the most potent MAO-B inhibitors belong to this class of compounds and that high SIs are also associated with many of them. In fact, compounds **22a**−**d** can be seen in the region of highly potent and selective inhibitors (i.e., in the lower right-hand corner of the plot in Figure 1).

The 4-*N*-methylaminomethyl derivatives **22b** and **22c**, bearing at position 7 a *m*-halogenosubstituted benzyloxy group, and the 4-aminomethyl-7-(*m*-clorobenzyloxy)coumarin derivative **24b** exhibited the highest MAO-B inhibitory potencies (IC_{50} of 13, 18, and 15 nM, respectively) and high SIs (457, 750, and 133, respectively). The presence of *N*-alkyl groups larger than the methyl group decreased the affinity (compare **22c** vs **22e** and **22f**, and **22b** vs **22g**). Similarly, *N*,*N*-dimethyl derivatives were less potent than the corresponding *N*-methyl analogues (compare **22a** vs **22h**, **22b** vs **22i**, and **22c** vs **22j**). A steric effect can be hypothesized around the position 4 as previously observed for the *N*-alkyl- and the *N*,*N*-dialkylcarboxamido derivatives (Table 2). The finding that the most hindered *N*,*N*-dialkylamine (**22k**) and *N*,*N*-dialkylcarboxamide (**21g**) derivatives yielded the lowest MAO-B affinity (IC_{50} of 8 and $> 10\ \mu M$) of the entire series of the two classes of examined inhibitors in Tables 2 and 3 might lend support to this hypothesis.

The short elongation of the aliphatic chain at position 4 of 7-*m*-chlorobenzyloxy derivatives **24b** and **22b** afforded compounds **26** and **30a**, respectively, exhibiting significantly lower MAO-B affinities.

Molecular Modeling Studies. The SAFIRs and SSRs discussed previously provided useful information on the main molecular determinants of the inhibitor potency and selectivity; however, a clear picture of the main interactions taking place at the binding sites of the two rat isoenzymes was still missing. A modeling study was therefore carried out through homology building and docking simulations for the purpose of (i) gaining insights on the nature and spatial location of the key interactions of the 4-substituents modulating the MAO-B affinity, (ii) explaining the excellent MAO-B selectivity observed for some classes of examined coumarins, and (iii) confirming, complementing, and better interpreting the results of previous studies conducted by our group on different sets of coumarin derivatives.[45,46]

Analysis of crystal structures of hMAO-B in complex with several inhibitors[6,36,56] revealed that the binding site consists of two cavities, the "substrate cavity" located near the FAD cofactor and the "entrance cavity", connected to the protein surface. The two cavities are separated by residues Tyr326, Ile199, Leu171 and Phe168, with Ile199 and Tyr326 behaving as gate-keeper residues. However, our attention was also drawn by other, apparently less important, structural features, i.e., the cocrystallized water molecules embedded in the reported X-ray complexes of hMAO-B. It is known that water molecules may become trapped in the protein crystal structure and, in addition, a number of them may contribute to the stabilization of the protein structure or of the protein−ligand complex through the formation of a network of hydrogen bonds bridging the ligand to specific binding site residues.[73,74] These structural water molecules are often conserved in crystallographic complexes of different ligands with the same macromolecular ligate and may play an important role in docking simulations and virtual screening.[75,76] Therefore, the detection of water molecules assuming a structural role in ligand binding is an important prerequisite to improve binding mode prediction of new ligands and the hit selection rate in docking virtual screening.[77,78] Accordingly, in a recent study of hMAO-B crystal structure (PDB code 1ojc),[46] we designated as structural water those molecules intercepting the energetic hot spots mapped on a grid through a water molecule probe available in GRID.[79] A minimum of four water molecules were assumed to be critical in the ligand binding with MAO-B. To our satisfaction, our findings were recently largely confirmed in a study based on the structural sampling of water molecules occurring in different PDB crystals released for hMAO-B.[39] Starting with these observations, we carried out an accurate analysis of the hMAO-B complex (PDB code 2v60) that included 11 water molecules within a sphere of 6 Å around the cocrystallized inhibitor, the 4-formyl-7-*m*-chlorobenzyloxycoumarin (4-FCBC). Campaigns of molecular docking simulations were then conducted to select among the 11 water molecules those influencing inhibitor binding. Such a selection was done comparing the accuracy of docking simulations in successfully reproducing

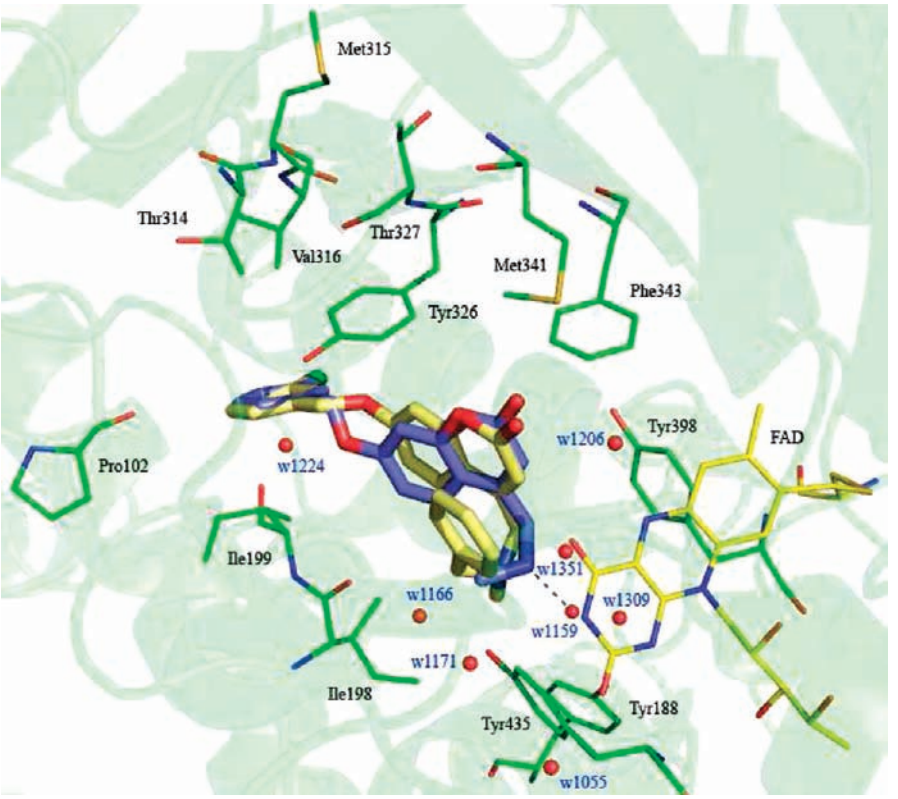

Figure 2. Docking poses of inhibitors **22b** and **22k** (rendered in yellow and cyan stick models, respectively) into rMAO-B binding site. Amino acid residues and FAD cofactor are represented in thin line form, colored according to the atom code (C atoms in green and yellow for amino acid residues and cofactor, respectively). Structural water molecules are represented as red balls. Hydrogen bonds are drawn as dark-blue dashed lines.

the binding mode of the cocrystallized 4-FCBC into hMAO-B binding site. As in previous studies, GOLD software was used in all the simulations. The best combination of water molecules, returning the lowest rmsd value of 0.578 Å with a docking score of 59.46 kJ/mol, included eight water molecules labeled as w1055, w1159, w1166, w1171, w1206, w1224, w1309, and w1351 according to the numbering reported in the cited hMAO-B X-ray complex. Given that our MAO inhibition data were determined on rat brain mitochondria assay, we first developed a 3D homology model of rat MAO-B for which no crystallographic data were available, starting from the rMAO-B sequence and the Cartesian coordinates of the PDB 2v60 complex. A proper fitting was also set for reconstructing the position in rMAO-B of both the FAD cofactor and the eight designated water molecules coming from the hMAO-B analysis. Confidence in the developed homology model was ensured by the high primary structure similarity (88%) and more so by the high degree of residue conservation into the binding site of rat and human enzymes. The cocrystallized 4-FCBC ligand of the 2v60 PDB structure did not exhibit appreciable binding differences with the hMAO-B when docked into the rMAO-B model. Only slight geometrical differences (rmsd = 0.855 Å) were observed without any remarkable change in the binding topology. In light of these encouraging results, the chemical scaffold of the best ranked solution of the coumarin inhibitor 4-FCBC docked into the rMAO-B was used to physically constrain the docking simulations of selected inhibitors. The constraint was limited to the 7-benzyloxy substituents that were found to always assume a preferred binding conformation into the hydrophobic binding site composed of Val316, Pro102, Tyr 326, Ile198, and Ile199 side chains. A visual inspection of Figures 2 and 3 revealed that the selected and docked inhibitors **22b** and **22k**, and **22c** and **22f**, respectively, adopted a convergent binding mode with the coumarin ring facing the FAD moiety and the lactonic carbonyl generally involved in a hydrogen bond with the hydroxyl group of Tyr398. In addition, it was found that while amides or amines with small *N*-alkyl substituents at position 4 of the coumarin ring were well accommodated into the protein binding site and the protonated nitrogen atoms formed hydrogen bonds with water molecules w1351, w1166, and w1159 affording high GoldScore values (59.86, 55.30, 53.35, and 65.70 kJ/mol, for **11b**, **22b**, **22c**, and **24b**, respectively), the presence of bulkier *N*-alkyl groups such as isopropyl (**22f**), *n*-butyl (**21c**), or benzyl (**22k**) decreased the capability of establishing valuable binding interactions with specific amino acid side chains and water molecules into the protein binding site, leading to significantly lower GoldScores values (45.38, 46.56, and 44.44 kJ/mol, respectively).

Although docking score energy was mainly related to hydrophobic interactions that should be increasingly relevant for larger groups, in our analysis no significant difference occurred when comparing van der Waals terms of coumarins substituted at position 4 with small (**22b** and **22c**) and large (**22k** and **22f**) substituents. A major propensity to form hydrogen bonds was instead observed in 4-substituted coumarins bearing small (**22b** and **22c**) rather than large (**22k** and **22f**) substituents as denoted by the values of the external hydrogen bond term. As unequivocally shown in Figures 2 and 3, inhibitors with large groups at position 4 adopted folded conformations, and this may distort the correct geometry for a strong hydrogen bond interaction

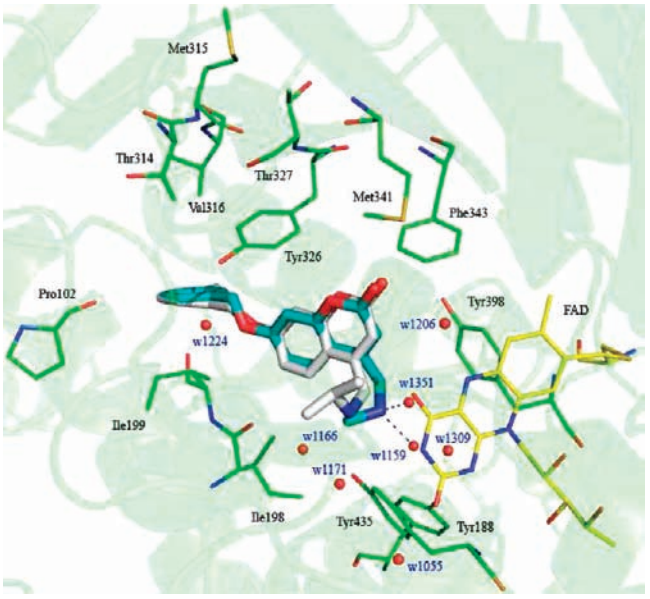

Figure 3. Docking poses of inhibitors **22c** and **22f** (rendered in light-blue and white stick models, respectively) into rMAO-B binding site. Amino acid residues and FAD cofactor are represented in thin line form, colored according to the atom code (C atoms in green and yellow for amino acid residues and cofactor, respectively). Structural water molecules are represented as red balls. Hydrogen bonds are drawn as dark-blue dashed lines.

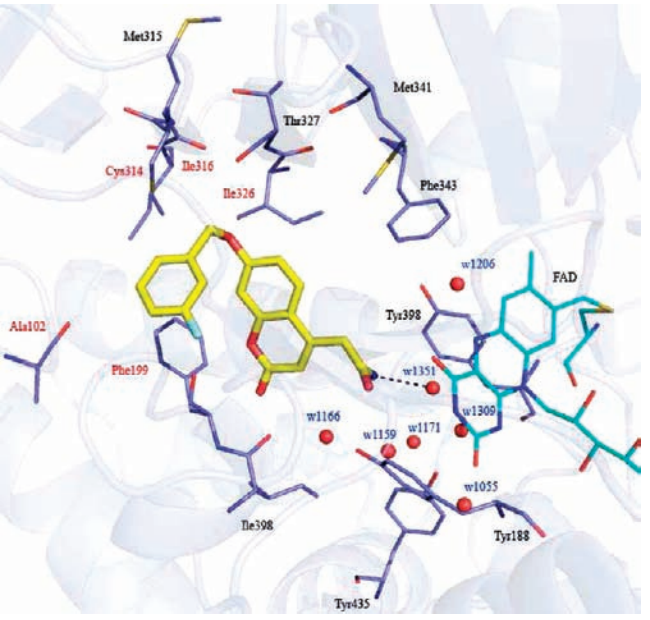

Figure 4. Top-score docking pose of inhibitor **11c**, rendered in yellow stick model, into rMAO-A binding site. Amino acid residues and FAD cofactor are represented in thin line form, colored according to the atom code (C atoms in blue and cyan for amino acid residues and cofactor, respectively). Structural water molecules are represented as red balls. Hydrogen bonds are drawn as dark-blue dashed lines. The different amino acids with respect to rMAO-B residues are labeled in magenta according to the numbering of rMAO-B.

between protonated nitrogens and surrounding water molecules. In addition, the analysis of GoldScore values attributed to each of the 10 top-scored poses per compound revealed a narrower standard deviation for both **22b** and **22c** (approximately ±4%) compared to both **22k** and **22f** (approximately ±6.5%). Finally, the energy gap between top and bottom scored docking solutions of **22b** and **22c** compared to **22k** and **22f** increased from about 13 to 29 kJ/mol. Taken together, all the above observations clearly indicated that large groups at position 4 can be accommodated only at the expense of high-energy inhibitor conformations unable to engage optimal ligand−protein interactions.

Interestingly, 4-substituted 7-(*m*-halogenobenzyloxy)coumarins exhibited generally higher docking scores compared to the corresponding unsubstituted benzyloxy derivatives, according to the experimental inhibition data.

Further analyses were carried out to investigate the reasons behind the pronounced selective inhibition of MAO-B exhibited by most of the coumarins analyzed. Given that only a low-resolution rMAO-A complex was available and water molecules were even missing (PDB code 1o5w), our investigation was focused on the hMAO-A/harmine complex (PDB code 2z5x). Rat and human MAO-A exhibited strong structural resemblance with an rmsd equal to 0.438 Å, a sequence similarity of 87%, and a binding site with identical amino acid residues. Interestingly, 7 out of the 8 selected water molecules for hMAO-B (w1055, w1159, w1166, w1171, w1206, w1309, and w1351) were also preserved in the hMAO-A binding site. These water molecules were therefore transferred into the rMAO-A crystal structure before running molecular docking simulations on a number of highly selective MAO-B inhibitors (i.e., **11c**, **11b**, **22a**, and **22c**). Because no MAO-A X-ray complex with coumarin ligands was available, the docking simulations were conducted without constraints. Not surprisingly, as shown in Figure 4, a diverse and somehow divergent binding mode was observed in both rMAO-A and rMAO-B. Moreover, in rMAO-A, a remarkable lowering of docking scores was generally found. For instance, for inhibitor **11c** a GoldScore of 19.92 kJ/mol was measured. The presence of diverse residues forming the entrance cavity of the rMAO-A compared to rMAO-B (i.e., Phe199Ile, Ala102Pro, Cys314Thr, Ile316Val and Ile326Tyr) is supposed to determine a different orientation of **11c**. As illustrated in Figure 4, a number of favorable hydrogen bonds and hydrophobic interactions was lost in rMAO-A compared to rMAO-B.

Binding, Physicochemical, and Biopharmacological Profiling of 22b Mesylate. Experimental MAO-B affinity and selectivity, as well as the estimated promising lipophilicity and aqueous solubility of the 7-(*m*-chlorobenzyloxy)-coumarin derivative **22b**, prompted a deeper in silico and experimental investigation of its physicochemical and biopharmacological profiles. Indeed, the X-ray crystallographic structure of the complex of **22b** with human MAO-B has been solved and published by the Mattevi group and our group 2 years ago[56] and the main inhibitor-enzyme binding interactions have been identified and discussed therein.

As for the physicochemical characterization of **22b**, aqueous solubility (*S*), pK_a, octanol−water partition coefficient (*P*), permeability coefficient (P_s, for passive oral absorption), blood−brain barrier permeability coefficient (LogBBB), and PSA, all relevant physicochemical parameters for drug dissolution, absorption, and distribution were experimentally or computationally determined.

Aqueous solubility of **22b**, assessed by the DMSO−buffer dilution turbidimetric method[63] at pH 7.4 and 3.0 was 52 μg/mL and 2.82 mg/mL, respectively, whereas pK_a and log *P* determined by potentiometric titration using the Sirius GLpKa instrument (Sirius Analytical Instruments Ltd.,

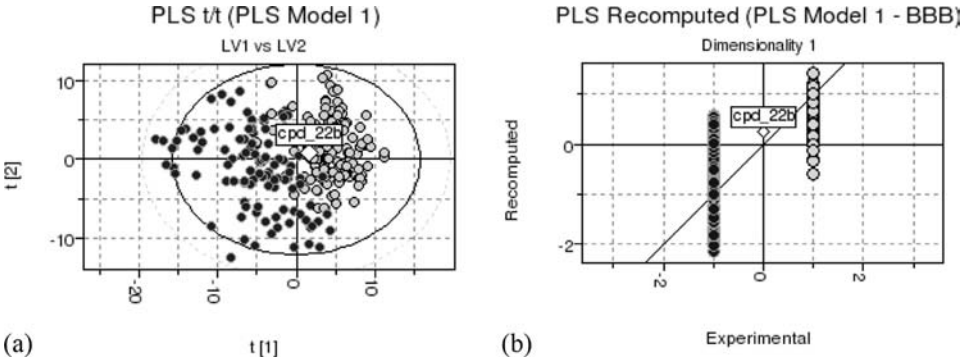

Figure 5. (a) Discriminant PLS t1−t2 analysis score plot for the BBB permeation model. BBB+ and BBB±/BBB− compounds are represented as dark and light solid gray circles respectively. Predicted compound **22b** is indicated by the solid white diamond. (b) Experimental vs predicted BBB values for model compound along with projection for the predicted **22b**.

Table 5. Permeability Data from HDM-PAMPA Assay

compd	R^a (%)	$C_A(t)/C_D(0)^b$ (%)	$\log P_e{}^c$
22b	10 ± 3	33.8 ± 0.3	−3.48 ± 0.01
3	72 ± 1	3.7 ± 0.3	−4.13 ± 0.10

[a] R = % of retention through the artificial membrane. [b] $C_A(t)/C_D(0)$ = % of compound that reaches the acceptor compartment. [c] P_e = effective permeability coefficient expressed in cm/s.

Forest Row, East Sussex, U.K.) were 7.18 ± 0.05 and 2.49 ± 0.03, respectively. PSA, another computational parameter used along with the rule of five of Lipinski to roughly estimate oral drug absorption,[66] was 49.8 Å^2, a value compatible with good biovailability and BBB permeation.[71]

Passive oral absorption of **22b**, was also evaluated experimentally by using the parallel artificial membrane permeability assay (PAMPA).[65,80] Experimental values of the retention through the artificial membrane (R, %), the quantity of compound reaching the acceptor compartment ($C_A(t)/C_D(0)$, %), and the effective permeability coefficient (P_e) of **22b** and **3** obtained using HDM-PAMPA are shown in Table 5. Both compounds presented a relatively high permeability coefficient through the hexadecane membrane. However, **3** was mostly retained in the membrane because of its notable affinity for hexadecane (as expected owing to its high log P predicted equal to 4.73 by Bioloom, Biobyte Corp., Claremont, CA). In contrast **22b** largely reached the acceptor compartment and was slightly retained in the artificial membrane.

The ability of **22b** to cross the BBB was assessed in silico through the estimation of the distribution parameter LogBBB from MIF-based Volsurf+ descriptors.[81] A LogBBB value of 0.386 was calculated for **22b**, a figure that was indicative of a good BBB permeation. Indeed, LogBBB values lower than −0.5 denote very poor brain permeation whereas values greater than 0.5 indicate high brain permeation.[82] To lend further support to the potentially good BBB permeation ability of **22b**, a knowledge-based approach was applied to a database containing a number of related, but chemically diverse, compounds exhibiting high, moderate, and poor BBB permeation (coded as BBB+, BBB±, and BBB−, respectively). After calculation of MIF-based Volsurf+ descriptors for the entire data set (245 compounds), y-response categorized variable was set to 1 for BBB+ compounds and to −1 for both BBB± and BBB− compounds. Partial least square discriminant analysis (PLS-DA)[83] was then carried out to develop a reliable BBB permeation model having confident statistics (r^2 = 0.708, q^2 = 0.659, SDEC = 0.538, SDEP = 0.582, PC = 3). As shown in Figure 5, the PLS t1−t2 score plot disclosed a good discrimination between the BBB+ on one side and BBB± and BBB− compounds on the other side. It was, in fact, immediately evident that the great majority of compounds was properly assigned to the correct class. On the basis of these solid statistics, the ability of **22b** to cross the BBB was evaluated with much confidence. To our satisfaction, **22b**, rendered as solid white diamond, was centered in the BBB+ region where CNS drugs are localized (Figure 5). It can therefore be assumed that **22b** is endowed with physicochemical properties that are typical of CNS drugs and that its choice for a further experimental biological characterization was appropriate.

Compared to the reference compound **3**, the aqueous solubility, lipophilicity, membrane and BBB permeability (log P_e and LogBBB, respectively), and the PSA of **22b** suggested a favorable profile for a CNS in vivo activity and prompted its in-depth biopharmacological profiling.

MAO-B inhibitory affinity of **22b** was therefore measured also in human PRP with a radioenzymatic assay using [^{14}C]PEA, a selective substrate already used in rat mitochondria. An IC_{50} of 3 nM, very close to that determined in the rat mitochondria assay (13 nM), was measured.

The reversible nature of MAO-B inhibition by **22b** was assessed in time-dependent inhibition experiments, by measuring the IC_{50} after 0 and 30 min of inhibitor−enzyme incubation (PRP as enzyme source). No significant difference between the IC_{50} with or without incubation was observed (6 vs 3 nM, respectively), as is typically detected with reversible inhibitors.

Subsequently, **22b** was also tested in ex vivo experiments as a selective MAO-B inhibitor. In C57Bl mice, 1 h after an oral or intraperitoneal dose of **22b** (3 mg/kg), brain MAO-B activity was almost completely inhibited while MAO-A was not affected (Figure 6).

In time-course experiments, following a 0.5 mg/kg oral dose of **22b**, MAO-B enzymatic activity was significantly inhibited at 30 min, 1 h, and 2 h (84%, 86%, and 90%, respectively), indicating a very rapid inhibition onset. Good MAO-B inhibition was maintained up to 8 h (nearly 60%), and full MAO-B activity was recovered after 16 h. During this time-course, MAO-A activity remained unchanged (Figure 7), suggesting that compound **22b** may be a tight binding inhibitor as lazabemide and safinamide. In a dose−response experiment, the ED_{50} for brain MAO-B inhibition, calculated 1 h after dose administration, was 0.24 mg/kg po (Figure 8).

To evaluate potential drug−drug interaction effects of **22b**, its inhibitory−induction activity on the selected series of

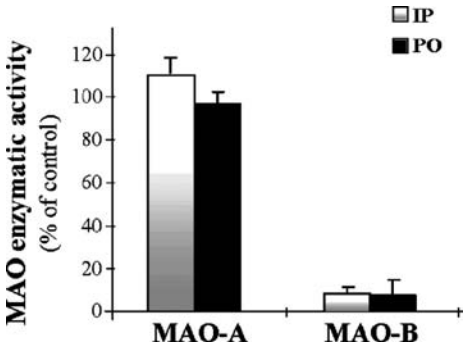

Figure 6. Ex vivo brain MAO activity after oral (po) and intraperitoneal administration (ip) of **22b** (3 mg/kg) in C57Bl mice. Mice (n = 6 per group) were treated (po or ip) with the test compound (3 mg/kg) and sacrificed after 1 h. The brains were removed, crude homogenates were prepared, and MAO enzyme activities were assessed with a radioenzymatic assay. Data were expressed as the mean ± SEM and were analyzed by ANOVA followed by Dunnett's test.

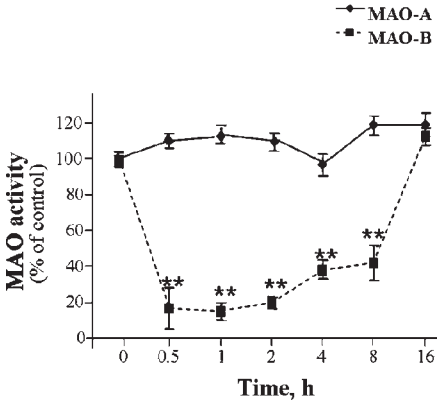

Figure 7. Ex vivo brain MAO activity after oral administration of **22b** (0.5 mg/kg) in C57Bl mice: time course experiment. Mice (n = 6 per group) were treated (po) with the test compound, and at different time intervals (0.5, 1, 2, 4, 8, and 16 h) they were sacrificed. The brains were removed, crude homogenates prepared and MAO enzyme activities assessed with a radioenzymatic assay. Data were expressed as the mean ± SEM and were analyzed by ANOVA followed by Dunnett's test.

recombinant human CYP450s was evaluated. Data revealed that **22b** inhibited the CYP450 isoforms at high micromolar concentrations with IC_{50} values between 5 and 50 μM. These data were quite promising, since compounds exhibiting $IC_{50} > 5-10\,\mu$M can be considered at low potential for drug−drug interaction because of the inhibition of CYP450 activity.

Finally, the in vitro effect of **22b** on SH-SY5Y cell viability was measured. As shown in Figure 9, incubation of cells for 24 h in a serumless medium containing **22b** did not induce any cellular damage up to 10 μM with IC_{50} = 29.7 μM, thus exhibiting very little in vitro toxicity.

Conclusions

A new class of higly potent and selective coumarin MAO-B inhibitors with an excellent biopharmacological profile was identified. SAFIRs and SSRs and modeling studies provided a clear picture of the main interactions taking place at position 4 of the newly designed 4,7-disubstituted coumarin derivatives and deepened our understanding of the structural requirements for high MAO-B affinity and selectivity. The determination or computational estimation of a number of physicochemical

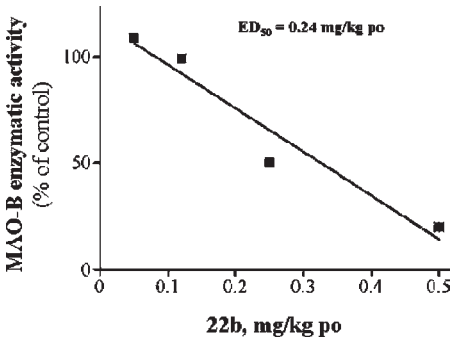

Figure 8. Ex vivo brain MAO activity after oral administration of **22b** (0.05, 0.1, 0.25, 0.5 mg/kg) in C57Bl mice: dose−response experiment. Mice (n = 6 per group) were treated with the test compound at different doses (0.05 − 0.5 mg/kg/po) and sacrificed after 1 h. The brains were removed, crude homogenates prepared, and MAO enzyme activities assessed with a radioenzymatic assay. Data were expressed as the mean ± SEM and were analyzed by ANOVA followed by Dunnett's test.

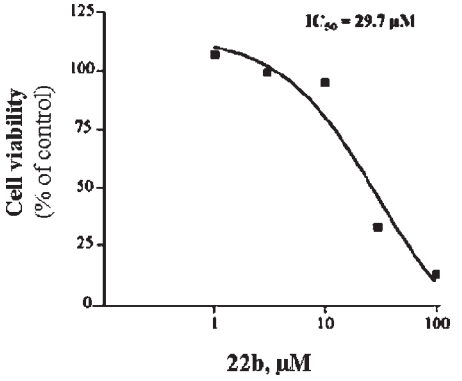

Figure 9. Effect of **22b** on SH-SY5Y cell viability.

parameters relevant for drug activity in vivo led us to select compound **22b** for an in-depth biopharmacological profiling. In vitro radioenzymatic assays in rat brain mitochondria and in human PRP showed that **22b** was a strong MAO-B inhibitor (IC_{50} of 13 and 3 nM, respectively) endowed with a high MAO-B selectivity (SI = 453, in rat brain mitochondria). The MAO-B inhibition of **22b** was not time-dependent as it would be for reversible inhibitors. In ex vivo experiments, **22b** showed an excellent BBB penetrating capacity when administered both parenterally and orally and behaved as a very potent (ED_{50} = 0.24 mg/kg po), reversible, and short-acting (full recovery of the enzymatic activity at 16 h) MAO-B inhibitor with no significant effect on MAO-A. Moreover, compound **22b** exhibited no CYP isoform liabilities and was devoided of cytotoxic effects.

Because of its excellent in vitro and in vivo MAO-B inhibitory activity and appropriate pharmacokinetic properties, compound **22b** may be considered as a promising clinical candidate for the therapy of neurodegenerative diseases and, analogous to selegeline,[20] for major depressive disorders.

Finally, we anticipate that compound **22b** also exhibits an interesting, albeit low, inhibitory activity toward acetylcholinesterase, an enzyme targeted by most of the anti-Alzheimer's drugs currently used in the therapy of this continuously growing neurodegenerative disease.[84] An improvement of AChE inhibitory activity, while maintaining a sufficiently strong MAO-B inhibitory potency, is an important goal of

our ongoing research addressing the preparation of multipotent ligands for the therapy of neurological disorders.[54,85]

Experimental Section

Chemistry. Starting materials and reagents (including **1e** and **5**), the resin for solid phase synthesis and analytical grade solvents were from commercial sources. Melting points were determined by the capillary method on a Stuart Scientific SMP3 electrothermal apparatus and are uncorrected. Elemental analyses were performed on the Euroea 3000 analyzer only on the final compounds tested as MAO inhibitors. The measured values for C, H, and N agreed to within ±0.40% of the theoretical values. The purity of the intermediates, checked by ^{1}H NMR and HPLC, was always better than 95%. IR spectra were recorded using potassium bromide disks on a Perkin-Elmer Spectrum One FT-IR spectrophotometer; only the most significant IR absorption bands are reported. ^{1}H NMR spectra were recorded in the specified deuterated solvent at 300 MHz on a Varian Mercury 300 instrument. Chemical shifts are expressed in parts per million (δ) relative to the solvent signal and the coupling constants J in hertz (Hz). The following abbreviations were used: s (singlet), d (doublet), t (triplet), q (quadruplet), dd (double doublet), m (multiplet), br (broad signal); signals due to OH or NH protons were located by deuterium exchange with D_2O. Chromatographic separations were performed on silica gel (230−400 mesh, Merck) by using the flash methodology.

Ethyl (7-Hydroxy-2-oxo-2*H*-chromen-4-yl)acetate (1a). Resorcinol (2.2 g, 20 mmol), diethyl 1,3-acetonedicarboxylate (4.0 mL, 22 mmol), and few drops of 96% sulfuric acid were stirred at 120 °C for 1 h. The oily residue obtained was crystallized from absolute ethanol, yielding a red solid (2.48 g, 50% yield). ^{1}H NMR (300 MHz, DMSO-d_6) δ: 1.16 (t, J = 7.1 Hz, 3H), 3.91 (s, 2H), 4.09 (q, J = 7.1 Hz, 2H), 6.21 (s, 1H), 6.71 (d, J = 2.3 Hz, 1H), 6.78 (dd, J_1 = 2.3 Hz, J_2 = 8.8 Hz, 1H), 7.49 (d, J = 8.8 Hz, 1H), 10.55 (br s, 1H). IR cm^{-1} (KBr): 3230, 1713, 1682, 1205, 1026, 849.

4-(Chloromethyl)-7-hydroxy-2*H*-chromen-2-one (1b). Resorcinol (10 g, 91 mmol) was dissolved in 100 mL of 96% sulfuric acid at 0 °C. Then ethyl 4-chloroacetoacetate (10 mL, 74 mmol) was slowly added and the mixture was stirred at 0−5 °C for 2 h. The reaction mixture was then poured onto ice−water (1000 g) and the solid was filtered and washed with water, yielding the desired coumarin as white solid (12.2 g, 78% yield). ^{1}H NMR (300 MHz, acetone-d_6) δ: 4.92 (s, 2H), 6.40 (s, 1H), 6.80 (d, J = 2.5 Hz, 1H), 6.91 (dd, J_1 = 2.5 Hz, J_2 = 8.8 Hz, 1H), 7.73 (d, J = 8.8 Hz, 1H), 9.50 (s, 1H, dis. with D_2O). IR cm^{-1} (KBr): 3283, 1686, 1235, 1136, 850.

4,7-Dihydroxy-2*H*-chromen-2-one (1c). Resorcinol (8.8 g, 80 mmol), malonic acid (25 g, 240 mmol), and 40 mL of boron trifluoride−diethyl etherate complex ($BF_3 \cdot Et_2O$) were mixed at 90 °C for 24 h under magnetic stirring. The crude mixture was poured onto crushed ice (300 g), and the resulting precipitate was filtered, washed with diethyl ether (50 mL), and then purified by column chromatography using as eluent the mixture $CHCl_3/CH_3OH$, 9.5/0.5 (v/v). Yield: 23%. ^{1}H NMR (300 MHz, DMSO-d_6) δ: 5.36 (s, 1H), 6.64 (d, J = 2.2 Hz, 1H), 6.75 (dd, J_1 = 2.2 Hz, J_2 = 8.8 Hz, 1H), 7.62 (d, J = 8.8 Hz, 1H), 10.51 (s, 1H, dis. in D_2O), 12.23 (s, 1H, dis. in D_2O). IR cm^{-1} (KBr): 1662, 1635, 1098, 802.

4-Chloro-7-hydroxy-2*H*-chromen-2-one (1d). An amount of 2.0 g (11 mmol) of **1c** was refluxed in 12 mL of $POCl_3$ for 4 h. The mixture was poured onto crushed ice (100 g), and the aqueous layer was extracted with ethyl acetate (3 × 40 mL). The organic phases were collected and dried over sodium sulfate, and the solvent was evaporated under reduced pressure. The resulting red oil was purified by flash chromatography (eluent *n*-hexane/ethyl acetate, 8/2 v/v), furnishing a red solid (995 mg, 46% yield). ^{1}H NMR (300 MHz, DMSO-d_6) δ: 6.60 (s, 1H), 6.76 (d, J = 2.2 Hz, 1H), 6.88 (dd, J_1 = 2.2 Hz, J_2 = 8.8 Hz, 1H), 7.69 (d, J = 8.8 Hz, 1H), 10.89 (s, 1H, dis. with D_2O). IR cm^{-1} (KBr): 1706, 1624, 1272, 841.

General Procedure for the Synthesis of Chlorides 2a−e. An amount of 4.6 mmol of **1b** or **1d** was dissolved in 45 mL of hot ethanol. Then potassium carbonate (0.63 g, 4.6 mmol) and 5.5 mmol of the appropriate benzyl bromide (0.65 mL of benzyl bromide in the case of **2a** and **2c**, 0.72 mL of 3-chlorobenzyl bromide in the case of **2b** and **2d**, 0.68 mL of 3-fluorobenzyl bromide in the case of **2e**) were added. The mixture was refluxed for 2 h and then cooled, and the inorganic residue was filtered off. The solvent was evaporated and the resulting solid was treated with diethyl ether and filtered, giving the desired products as off-white solids.

7-(Benzyloxy)-4-chloro-2*H*-chromen-2-one (2a). Yield: 55%. ^{1}H NMR (300 MHz, $CDCl_3$) δ: 5.15 (s, 2H), 6.43 (s, 1H), 6.89 (d, J = 2.2 Hz, 1H), 6.99 (dd, J_1 = 2.2 Hz, J_2 = 9.1 Hz, 1H), 7.34−7.44 (m, 5H), 7.75 (d, J = 9.1 Hz, 1H). IR cm^{-1} (KBr): 1735, 1359, 1126, 833.

4-Chloro-7-[(3-chlorobenzyl)oxy]-2*H*-chromen-2-one (2b). Yield: 68%. ^{1}H NMR (300 MHz, $CDCl_3$) δ: 5.12 (s, 2H), 6.45 (s, 1H), 6.87 (d, J = 2.5 Hz, 1H), 6.99 (dd, J_1 = 2.5 Hz, J_2 = 9.1 Hz, 1H), 7.30−7.38 (m, 3H), 7.44 (s, 1H), 7.78 (d, J = 9.1 Hz, 1H). IR cm^{-1} (KBr): 1721, 1365, 1275, 865, 838.

7-(Benzyloxy)-4-(chloromethyl)-2*H*-chromen-2-one (2c). Yield: 69%. ^{1}H NMR (300 MHz, $CDCl_3$) δ: 4.62 (s, 2H), 5.14 (s, 2H), 6.40 (s, 1H), 6.92 (d, J = 2.5 Hz, 1H), 6.97 (dd, J_1 = 2.5 Hz, J_2 = 8.8 Hz, 1H), 7.34−7.45 (m, 5H), 7.57 (d, J = 8.8 Hz, 1H). IR cm^{-1} (KBr): 1732, 1615, 1396, 1264, 1199, 1057, 1008.

7-[(3-Chlorobenzyl)oxy]-4-(chloromethyl)-2*H*-chromen-2-one (2d). Yield: 78%. ^{1}H NMR (300 MHz, $CDCl_3$) δ: 4.62 (s, 2H), 5.11 (s, 2H), 6.41 (s, 1H), 6.88 (d, J = 2.5 Hz, 1H), 6.96 (dd, J_1 = 2.5 Hz, J_2 = 8.8 Hz, 1H), 7.27−7.37 (m, 3H), 7.43 (br s, 1H), 7.58 (d, J = 8.8 Hz, 1H). IR cm^{-1} (KBr): 1699, 1611.

4-(Chloromethyl)-7-[(3-fluorobenzyl)oxy]-2*H*-chromen-2-one (2e). Yield: 73%. ^{1}H NMR (300 MHz, $CDCl_3$) δ: 4.62 (s, 2H), 5.14 (s, 2H), 6.41 (s, 1H), 6.89 (d, J = 2.5 Hz, 1H), 6.97 (dd, J_1 = 2.5 Hz, J_2 = 8.8 Hz, 1H), 7.01−7.07 (m, 1H), 7.13−7.25 (m, 2H), 7.34−7.41 (m, 1H), 7.58 (d, J = 8.8 Hz, 1H). IR cm^{-1} (KBr): 1718, 1611.

7-(1,3-Benzodioxol-5-ylmethoxy)-4-(chloromethyl)-2*H*-chromen-2-one (2f). An amount of 1.0 mmol (0.21 g) of **1b** was dissolved in 10 mL of anhydrous THF. Piperonyl alcohol (0.46 g, 3.0 mmol), DIAD (0.59 mL, 3.0 mmol), and PPh_3 (0.79 g, 3.0 mmol) were added, and the mixture was stirred at room temperature for 18 h. The solvent was removed under vacuum, and the resulting crude oil was purified by column chromatography using as eluent a mixture of chloroform/petroleum ether, 1/1 (v/v). Yield: 76%. ^{1}H NMR (300 MHz, $CDCl_3$) δ: 4.62 (s, 2H), 5.03 (s, 2H), 5.98 (s, 2H), 6.40 (s, 1H), 6.79−6.84 (m, 2H), 6.87−6.91 (m, 2H), 6.93−6.96 (m, 1H), 7.55−7.58 (m, 1H). IR cm^{-1} (KBr): 1731, 1614.

7-[(3-Chlorobenzyl)oxy]-4-methyl-2*H*-chromen-2-one (3). An amount of 0.81 g (4.6 mmol) of commercially available **1e** was dissolved in 45 mL of hot ethanol. Then potassium carbonate (0.63 g, 4.6 mmol) and 3-chlorobenzyl bromide (0.72 mL, 5.5 mmol) were added. The mixture was refluxed for 2 h and then cooled. The inorganic residue was filtered off and the product crystallized from the resulting solution. Yield: 88%. Mp: 148−9 °C. ^{1}H NMR (300 MHz, $CDCl_3$) δ: 2.40 (d, J = 1.1 Hz, 3H), 5.10 (s, 2H), 6.15 (d, J = 1.1 Hz, 1H), 6.86 (d, J = 2.5 Hz, 1H), 6.93 (dd, J_1 = 2.5 Hz, J_2 = 8.8 Hz, 1H), 7.28−7.37 (m, 3H), 7.44 (s, 1H), 7.51 (d, J = 8.8 Hz, 1H). IR cm^{-1} (KBr): 1713, 1614. Anal. ($C_{17}H_{13}ClO_3$) C, H.

General Procedure for the Synthesis of Coumarin Amines 4a−h. An amount of 0.50 mmol of the appropriate chloro derivative **2a−e** was dissolved in 4.0 mL of dry DMF. Then 0.26 mL (1.5 mmol) of DIEA and 0.75 mmol of the appropriate amino acid (for compounds **4a**,**b**,**f**, 0.093 g of L-alaninamide hydrochloride; for compound **4c**,**d**,**g**,**h**, 0.086 g of L-prolinamide; for compound **4e**, 0.11 g of L-serinamide hydrochloride) were added, and the mixture was stirred at 80 °C for 5 h. The solvent

was evaporated, and the resulting crude was purified by column chromatography (eluent $CHCl_3/CH_3OH$, 9.5/0.5 v/v).

***N*²-[7-(Benzyloxy)-2-oxo-2*H*-chromen-4-yl]alaninamide (4a).** Yield: 77%. Mp: 247−9 °C. ^{1}H NMR (300 MHz, DMSO-d_6) δ: 1.42 (d, J = 6.9 Hz, 3H), 3.97−4.01 (m, 1H), 4.88 (s, 1H), 5.19 (s, 2H), 6.94 (d, J = 2.2 Hz, 1H), 6.99 (dd, J_1 = 2.2 Hz, J_2 = 9.1 Hz, 1H), 7.30−7.47 (m, 6H), 7.17 (s, 1H), 7.61 (s, 1H), 8.12 (d, J = 9.1 Hz, 1H). IR cm^{-1} (KBr): 3325, 1668, 1609. Anal. ($C_{19}H_{18}N_2O_4$) C, H, N.

***N*²-{7-[(3-Chlorobenzyl)oxy]-2-oxo-2*H*-chromen-4-yl}alaninamide (4b).** Yield: 82%. Mp: 237−9 °C. ^{1}H NMR (300 MHz, DMSO-d_6) δ: 1.42 (d, J = 6.9 Hz, 3H), 3.97−4.01 (m, 1H), 4.88 (s, 1H), 5.21 (s, 2H), 6.95 (d, J = 2.2 Hz, 1H), 7.00 (dd, J_1 = 2.2 Hz, J_2 = 9.1 Hz, 1H), 7.17 (s, 1H), 7.39−7.44 (m, 4H), 7.54 (s, 1H), 7.62 (s, 1H), 8.13 (d, J = 9.1 Hz, 1H). IR cm^{-1} (KBr): 3437, 3180, 1674, 1613. Anal. ($C_{19}H_{17}ClN_2O_4$) C, H, N.

1-[7-(Benzyloxy)-2-oxo-2*H*-chromen-4-yl]prolinamide (4c). Yield: 59%. Mp: 203−5 °C. ^{1}H NMR (300 MHz, DMSO-d_6) δ: 1.82−1.99 (m, 3H), 2.26−2.30 (m, 1H), 3.78−3.79 (m, 1H), 3.92−4.00 (m, 1H), 4.29−4.34 (m, 1H), 4.91 (s, 1H), 5.20 (s, 2H), 6.92 (dd, J_1 = 2.8 Hz, J_2 = 9.1 Hz, 1H), 6.97 (d, J = 2.8 Hz, 1H), 7.21 (s, 1H), 7.31−7.47 (m, 5H), 7.67 (s, 1H), 7.95 (d, J = 9.1 Hz, 1H). IR cm^{-1} (KBr): 3475, 3195, 1691, 1669, 1615. Anal. ($C_{21}H_{20}N_2O_4$) C, H, N.

1-{7-[(3-Chlorobenzyl)oxy]-2-oxo-2*H*-chromen-4-yl}prolinamide (4d). Yield: 73%. Mp: 222−3 °C. ^{1}H NMR (300 MHz, DMSO-d_6) δ: 1.82−1.99 (m, 3H), 2.26−2.27 (m, 1H), 3.73−3.78 (m, 1H), 3.94−3.97 (m, 1H), 4.29−4.32 (m, 1H), 4.91 (s, 1H), 5.22 (s, 2H), 6.93 (dd, J_1 = 2.8 Hz, J_2 = 9.1 Hz, 1H), 6.97 (d, J = 2.8 Hz, 1H), 7.19 (s, 1H), 7.40−7.44 (m, 3H), 7.53 (s, 1H), 7.66 (s, 1H), 7.95 (d, J = 9.1 Hz, 1H). IR cm^{-1} (KBr): 3478, 3193, 1688, 1669, 1615. Anal. ($C_{21}H_{19}ClN_2O_4$) C, H, N.

***N*²-{7-[(3-Chlorobenzyl)oxy]-2-oxo-2*H*-chromen-4-yl}serinamide (4e).** Yield: 48%. Mp: 244 °C (dec). ^{1}H NMR (300 MHz, DMSO-d_6) δ: 3.75−3.80 (m, 2H), 3.96−4.02 (m, 1H), 4.94 (d, J = 1.9 Hz, 1H), 5.05−5.09 (m, 1H), 5.22 (s, 2H), 6.96 (d, J = 2.5 Hz, 1H), 7.02 (dd, J_1 = 2.5 Hz, J_2 = 9.1 Hz, 1H), 7.23 (d, J = 6.9 Hz, 1H), 7.26 (s, 1H), 7.38−7.43 (m, 3H), 7.54 (s, 1H), 7.64 (s, 1H), 8.08 (d, J = 9.1 Hz, 1H). IR cm^{-1} (KBr): 3368, 3275, 3188, 1658, 1618. Anal. ($C_{19}H_{17}ClN_2O_5$) C, H, N.

***N*²-{[7-(Benzyloxy)-2-oxo-2*H*-chromen-4-yl]methyl}alaninamide (4f).** Yield: 63%. Mp: 151−3 °C. ^{1}H NMR (300 MHz, DMSO-d_6) δ: 1.23 (d, J = 6.6 Hz, 3H), 3.23−3.33 (m, 1H), 3.98−4.01 (m, 2H), 5.21 (s, 2H), 6.37 (s, 1H), 7.01 (dd, J_1 = 2.5 Hz, J_2 = 9.1 Hz, 1H), 7.07 (d, J = 2.5 Hz, 1H), 7.13 (br s, 1H), 7.33−7.47 (m, 6H), 7.73 (d, J = 9.1 Hz, 1H), 1NH not detectable. IR cm^{-1} (KBr): 3203, 1705, 1639, 1614. Anal. ($C_{20}H_{20}N_2O_4$) C, H, N.

1-{[7-(Benzyloxy)-2-oxo-2*H*-chromen-4-yl]methyl}prolinamide (4g). Yield: 74%. Mp: 67−9 °C. ^{1}H NMR (300 MHz, DMSO-d_6) δ: 1.72−1.78 (m, 3H), 2.02−2.06 (m, 1H), 2.25−2.30 (m, 1H), 3.02−3.10 (m, 2H), 3.63 (d, J = 15.4 Hz, 1H), 3.93 (d, J = 15.4 Hz, 1H), 5.21 (s, 2H), 6.44 (s, 1H), 6.98 (dd, J_1 = 2.2 Hz, J_2 = 8.8 Hz, 1H), 7.06 (d, J = 2.2 Hz, 1H), 7.20 (s, 2H), 7.30−7.47 (m, 5H), 7.93 (d, J = 8.8 Hz, 1H). IR cm^{-1} (KBr): 3328, 3194, 1723, 1677, 1611. Anal. ($C_{22}H_{22}N_2O_4$) C, H, N.

1-({7-[(3-Fluorobenzyl)oxy]-2-oxo-2*H*-chromen-4-yl}methyl)-prolinamide (4h). Yield: 61%. Mp: 162−4 °C. ^{1}H NMR (300 MHz, DMSO-d_6) δ: 1.72 (br s, 3H), 1.98−2.08 (m, 1H), 2.25−2.33 (m, 1H), 3.01−3.10 (m, 2H), 3.63 (d, J = 15.4 Hz, 1H), 3.93 (d, J = 15.4 Hz, 1H), 5.23 (s, 2H), 6.44 (s, 1H), 6.97−7.05 (m, 3H), 7.13−7.31 (m, 4H), 7.40−7.47 (m, 1H), 7.95 (d, J = 8.8 Hz, 1H). IR cm^{-1} (KBr): 3193, 1739, 1649, 1613. Anal. ($C_{22}H_{21}FN_2O_4$) C, H, N.

Synthesis of Amides 6a,b. The commercially available 7-hydroxycoumarin-4-acetic acid **5** (0.44 g, 2.0 mmol) and HOBt (0.63 g, 4.0 mmol) were dissolved in 12 mL of anhydrous DMF. DCC (0.8 g, 4.0 mmol) was added followed by an amount of 4.0 mmol of *tert*-butyl carbazate (for **6a**) or *N*-Boc-ethylenediamine (for **6b**). The mixture was then stirred at room temperature for 5 h.

***tert*-Butyl 2-[(7-Hydroxy-2-oxo-2*H*-chromen-4-yl)acetyl]hydrazinecarboxylate (6a).** Yield: 98%. ^{1}H NMR (300 MHz, DMSO-d_6) δ: 1.40 (s, 9H), 3.60 (s, 2H), 6.22 (s, 1H), 6.70 (d, J = 2.4 Hz, 1H), 6.77 (dd, J_1 = 2.4 Hz, J_2 = 8.7 Hz, 1H), 7.61 (d, J = 8.7 Hz, 1H), 8.85 (s, 1H), 9.93 (s, 1H), 10.57 (s, 1H). IR cm^{-1} (KBr): 3302, 3206, 1727, 1705, 1683, 1607.

***tert*-Butyl 2-{[(7-Hydroxy-2-oxo-2*H*-chromen-4-yl)acetyl]-amino}ethylcarbamate (6b).** Yield: 65%. ^{1}H NMR (300 MHz, DMSO-d_6) δ: 1.35 (s, 9H), 2.96−3.05 (m, 4H), 3.60 (s, 2H), 6.14 (s, 1H), 6.69−6.78 (m, 3H), 7.57 (d, J = 8.8 Hz, 1H), 8.19 (br s, 1H), 10.54 (br s, 1H). IR cm^{-1} (KBr): 3360, 3335, 1695, 1680, 1656.

Synthesis of Amides 7a−c. The appropriate intermediate **6a**,**b** (1.5 mmol) was dissolved in absolute ethanol (10 mL) and K_2CO_3 (0.21 g, 1.5 mmol), and the suitable benzyl bromide (1.5 mmol) was added to the solution. The mixture was refluxed for 30 min. The solid was filtered off and the solution cooled at room temperature. The solvent was evaporated to give a solid that was purified by column chromatography (eluent $CHCl_3$/MeOH, 9.5/0.5 v/v).

***tert*-Butyl 2-{[7-(Benzyloxy)-2-oxo-2*H*-chromen-4-yl]acetyl}-hydrazinecarboxylate (7a).** Yield: 30%. ^{1}H NMR (300 MHz, DMSO-d_6) δ: 1.37 (s, 9H), 3.68 (s, 2H), 5.22 (s, 2H), 6.30 (s, 1H), 7.01 (dd, J_1 = 2.2 Hz, J_2 = 8.8 Hz, 1H), 7.08 (d, J = 2.2 Hz, 1H), 7.30−7.46 (m, 5H), 7.70 (d, J = 8.8 Hz, 1H), 8.85 (s, 1H), 9.94 (s, 1H). IR cm^{-1} (KBr): 3371, 3262, 1754, 1670.

***tert*-Butyl 2-{[7-(3-Chlorobenzyl)oxy)-2-oxo-2*H*-chromen-4-yl]-acetyl}hydrazinecarboxylate (7b).** Yield: 56%. ^{1}H NMR (300 MHz, DMSO-d_6) δ: 1.37 (s, 9H), 3.68 (s, 2H), 5.22 (s, 2H), 6.30 (s, 1H), 7.01 (dd, J_1 = 2.2 Hz, J_2 = 8.8 Hz, 1H), 7.08 (d, J = 2.2 Hz, 1H), 7.39−7.40 (m, 3H), 7.51 (s, 1H), 7.70 (d, J = 8.8 Hz, 1H), 8.85 (s, 1H), 9.94 (s, 1H). IR cm^{-1} (KBr): 3366, 3259, 1755, 1683.

***tert*-Butyl 2-[({7-[(3-Chlorobenzyl)oxy]-2-oxo-2*H*-chromen-4-yl}-acetyl)amino]ethylcarbamate (7c).** Yield: 95%. ^{1}H NMR (300 MHz, DMSO-d_6) δ: 1.35 (s, 9H), 2.94−2.98 (m, 2H), 3.03−3.07 (m, 2H), 3.64 (s, 2H), 5.23 (s, 2H), 6.23 (s, 1H), 6.81 (br s, 1H), 7.03 (dd, J_1 = 2.5 Hz, J_2 = 8.8 Hz, 1H), 7.07 (d, J = 2.5 Hz, 1H), 7.39−7.41 (m, 3H), 7.53 (s, 1H), 7.67 (d, J = 8.8 Hz, 1H), 8.21 (br s, 1H). IR cm^{-1} (KBr): 3356, 3290, 1729, 1685.

Synthesis of Amides 8a−c. The appropriate intermediate **7a−c** (0.060 mmol) was dissolved in 1.0 mL of a 1/1 v/v mixture of CH_2Cl_2/CF_3COOH and the solution stirred at room temperature for 20 min. The solvent was evaporated under vacuum and the oily residue obtained was treated with ether to give a precipitate that was filtered and crystallized from ethanol (**8a**,**b**) or chloroform/*n*-hexane (**8c**).

2-[7-(Benzyloxy)-2-oxo-2*H*-chromen-4-yl]acetohydrazide (8a). Yield: 93%. Mp: 164 °C (dec). ^{1}H NMR (300 MHz, DMSO-d_6) δ: 3.60 (s, 2H), 4.29 (br s, 2H, dis. with D_2O), 5.22 (s, 2H), 6.23 (s, 1H), 7.02 (dd, J_1 = 2.5 Hz, J_2 = 8.8 Hz, 1H), 7.07 (d, J = 2.5 Hz, 1H), 7.30−7.47 (m, 5H), 7.70 (d, J = 8.8 Hz, 1H), 9.31 (s, 1H, dis. with D_2O). IR cm^{-1} (KBr): 3303, 1716, 1644, 1615. Anal. ($C_{18}H_{16}N_2O_4$) C, H, N.

2-[7-(3-Chlorobenzyloxy)-2-oxo-2*H*-chromen-4-yl]acetohydrazide (8b). Yield: 86%. Mp 174−6 °C. ^{1}H NMR (300 MHz, DMSO-d_6) δ: 3.61 (s, 2H), 4.43 (br s, 2H, dis. with D_2O), 5.24 (s, 2H), 6.24 (s, 1H), 7.03−7.06 (m, 1H), 7.07 (br s, 1H), 7.41−7.42 (m, 3H), 7.53 (s, 1H), 7.71 (d, J = 8.8 Hz, 1H), 9.34 (s, 1H, dis. with D_2O). IR cm^{-1} (KBr): 3309, 1719, 1646. Anal. ($C_{18}H_{15}ClN_2O_4$) C, H, N.

***N*-(2-Aminoethyl)-2-{7-[(3-chlorobenzyl)oxy]-2-oxo-2*H*-chromen-4-yl}acetamide (8c).** Yield: 83%. Mp: 144−5 °C. ^{1}H NMR (300 MHz, DMSO-d_6) δ: 2.81−2.83 (m, 2H), 3.26−3.28 (m, 2H), 3.69 (s, 2H), 5.23 (s, 2H), 6.25 (s, 1H), 7.03 (dd, J_1 = 2.5 Hz, J_2 = 8.8 Hz, 1H), 7.09 (d, J = 2.5 Hz, 1H), 7.39−7.42 (m, 3H), 7.53 (s, 1H), 7.68 (d, J = 8.8 Hz, 1H), 7.74 (br s, 2H, dis. with D_2O), 8.33 (br s, 1H). IR cm^{-1} (KBr): 3356, 3290, 1700, 1683. Anal. ($C_{20}H_{19}ClN_2O_4$) C, H, N.

Solid-Phase Synthesis of Amides 11a−d and 13a,b. Resin 9. An amount of 0.060 mmol (0.10 g) of Rink amide AM resin was suspended in 2.0 mL of anhydrous DMF and shaken for 20 min. The swelled resin was suspended in 2.0 mL of a 20% solution of piperidine in anhydrous DMF and shaken for 30 min, filtered, and washed with anhydrous DMF (3 × 3.0 mL). The deprotected resin was suspended in 2 mL of anhydrous DMF, and 7-hydroxycoumarin-4-acetic acid **5** (0.070 g, 0.32 mmol), hydroxybenzotriazole (0.049 g, 0.32 mmol), and *N*,*N*-diisopropylcarbodiimide (0.050 mL, 0.32 mmol) were added. The mixture was shaken overnight. The resin was filtered and washed with DMF (3 × 2.0 mL) and THF (3 × 2.0 mL).

Resins 10a−d. An amount of 0.20 mmol (0.30 g) of resin-bound **9** was suspended in 4.0 mL of anhydrous DMF and shaken for 20 min. The swelled resin was suspended in 3.0 mL of anhydrous DMF. Then 1.9 mmol of the appropriate benzyl bromide (benzyl bromide for **10a**, 3-chlorobenzyl bromide for **10b**, 3-fluorobenzyl bromide for **10c**, and **17** for **10d**) and 0.34 mL (1.9 mmol) of DIEA were added. The shaking was continued at 70 °C for 2.5 h. The mixture was cooled at room temperature, the resin was filtered, washed with anhydrous DMF (3 × 3.0 mL), and the coupling was repeated in the same conditions. The mixture was filtered, and the resin was washed with DMF (3 × 3.0 mL), THF (3 × 3.0 mL), and dichloromethane (3 × 3.0 mL).

Resin 10e. An amount of 0.17 mmol of swelled resin **10d** was suspended in 2.0 mL of anhydrous THF, and 0.13 mL of saturated solution in methanol of sodium methoxide was added. The mixture was shaken for 4 h, filtered, and washed with THF/H_2O, 1/1 v/v (3 × 2.0 mL), THF/HCl 2.0 N, 1/1 v/v (3 × 2.0 mL), THF/H_2O, 1/1 v/v (3 × 2.0 mL), THF (3 × 2.0 mL), and CH_2Cl_2 (3 × 2.0 mL).

Resins 12a,b. An amount of 0.18 mmol of the resin **10a** (for **12a**) or **10c** (for **12b**) was suspended in 3.0 mL of anhydrous DMF and shaken for 20 min. The swelled resin was suspended in 2.0 mL of anhydrous DMF, and an amount of 1.1 mL (0.55 mmol) of a 0.5 M solution of KHMDS in toluene was added. The mixture was shaken for 10 min. The resin was filtered, washed with anhydrous DMF, resuspended in 2.0 mL of anhydrous DMF, and methyl iodide (0.23 mL, 3.7 mmol) was added. The resin was shaken for 4 h, filtered, and washed with DMF (3 × 2.0 mL), THF (3 × 2.0 mL), and CH_2Cl_2 (3 × 2.0 mL).

General Procedure for the Cleavage of Amides 11a−d and 13a,b. The functionalized resin **12a**,**b** or **10a−c** or **10e** was suspended in 3.0 mL of a 95% CF_3COOH, 2.5% H_2O, and 2.5% triethylsilane solution and shaken for 1 h. The resin was filtered and washed with the same solution (3 × 3.0 mL) and the solvent was evaporated under vacuum to give an oil that was treated with toluene, yielding a solid that was crystallized from ethanol or purified by column chromatography.

2-[7-(Benzyloxy)-2-oxo-2*H*-chromen-4-yl]acetamide (11a). Crystallized from ethanol. Yield: 53%. Mp: 218−221 °C (dec). ^{1}H NMR (300 MHz, DMSO-d_6) δ: 3.63 (s, 2H), 5.21 (s, 2H), 6.24 (s, 1H), 7.02−7.08 (m, 2H), 7.17 (s, 1H), 7.30−7.47 (m, 5H), 7.65−7.68 (m, 2H). IR cm^{-1} (KBr): 3395, 3305, 1713, 1661, 1612. Anal. ($C_{18}H_{15}NO_4$) C, H, N.

2-{7-[(3-Chlorobenzyl)oxy]-2-oxo-2*H*-chromen-4-yl}acetamide (11b). Purified by column chromatography (eluent: $CHCl_3$/MeOH, 9.5/0.5 v/v). Yield: 30%. Mp: 185−6 °C. ^{1}H NMR (300 MHz, DMSO-d_6) δ: 3.64 (s, 2H), 5.24 (s, 2H), 6.25 (s, 1H), 7.03−7.09 (m, 2H), 7.17 (s, 1H), 7.38−7.44 (m, 3H), 7.54 (s, 1H), 7.63 (s, 1H), 7.68 (d, J = 8.7 Hz, 1H). IR cm^{-1} (KBr): 3447, 3341, 1733, 1693, 1618. Anal. ($C_{18}H_{14}ClNO_4$) C, H, N.

2-{7-[(3-Fluorobenzyl)oxy]-2-oxo-2*H*-chromen-4-yl}acetamide (11c). Purified by column chromatography (eluent: $CHCl_3$/MeOH, 9.5/0.5 v/v). Yield: 44%. Mp: 177−8 °C. ^{1}H NMR (300 MHz, DMSO-d_6) δ: 3.63 (s, 2H), 5.24 (s, 2H), 6.24 (s, 1H), 7.03−7.07 (m, 2H), 7.13−7.17 (m, 2H), 7.29 (d, J = 7.7 Hz, 2H), 7.40−7.47 (m, 1H), 7.64 (s, 1H), 7.68 (d, J = 8.8 Hz, 1H). IR cm^{-1} (KBr): 3415, 1717, 1667, 1614. Anal. ($C_{18}H_{14}FNO_4$) C, H, N.

2-{7-[(3-Hydroxybenzyl)oxy]-2-oxo-2*H*-chromen-4-yl}acetamide (11d). Purified by column chromatography (eluent: CH_2Cl_2/MeOH, 8.5/1.5 v/v). Yield: 30%. Mp: 190−1 °C (dec). ^{1}H NMR (300 MHz, DMSO-d_6) δ: 3.62 (s, 2H), 5.13 (s, 2H), 6.23 (s, 1H), 6.68−6.70 (m, 1H), 6.81−6.85 (m, 2H), 6.99−7.18 (m, 4H), 7.63−7.66 (m, 2H), 9.51 (s, 1H). IR cm^{-1} (KBr): 3373, 3198, 1698, 1672, 1607. Anal. ($C_{18}H_{15}NO_5$) C, H, N.

2-[7-(Benzyloxy)-2-oxo-2*H*-chromen-4-yl]propanamide (13a). Crystallized from ethanol. Yield: 34%. Mp: 196 °C (dec), 204−6 °C. ^{1}H NMR (300 MHz, DMSO-d_6) δ: 1.38 (d, J = 7.2 Hz, 3H), 3.99 (q, J = 7.2 Hz, 1H), 5.21 (s, 2H), 6.19 (s, 1H), 7.04 (dd, J_1 = 2.5 Hz, J_2 = 8.8 Hz, 1H), 7.08 (d, J = 2.5 Hz, 1H), 7.14 (s, 1H), 7.32−7.46 (m, 5H), 7.59 (s, 1H), 7.76 (d, J = 8.8 Hz, 1H). IR cm^{-1} (KBr): 3398, 1716, 1667, 1618. Anal. ($C_{19}H_{17}NO_4$) C, H, N.

2-{7-[(3-Fluorobenzyl)oxy]-2-oxo-2*H*-chromen-4-yl}propanamide (13b). Crystallized from ethanol. Yield: 24%. Mp: 168−9 °C. ^{1}H NMR (300 MHz, DMSO-d_6) δ: 1.38 (d, J = 6.9 Hz, 3H), 3.99 (q, J = 6.9 Hz, 1H), 5.24 (s, 2H), 6.20 (s, 1H), 7.03−7.19 (m, 4H), 7.28−7.30 (m, 2H), 7.44 (dd, J_1 = 7.4 Hz, J_2 = 7.7 Hz, 1H), 7.59 (s, 1H), 7.77 (d, J = 8.5 Hz, 1H). IR cm^{-1} (KBr): 3422, 1723, 1655, 1618. Anal. ($C_{19}H_{16}FNO_4$) C, H, N.

3-Methylphenyl Benzoate (16). An amount of 1.0 mL (10 mmol) of *m*-cresol **14** and 7.0 mL (50 mmol) of anhydrous triethylamine were dissolved in 10 mL of anhydrous THF. Then 1.2 mL (10 mmol) of benzoyl chloride **15**, previously dissolved in 10 mL of anhydrous THF, were added dropwise at 0 °C. The mixture was stirred at room temperature for 30 min. The obtained precipitate was filtered and the solvent was evaporated under vacuum to give an oil that was purified by flash chromatography (eluent $CHCl_3$/*n*-hexane, 1/1 v/v). Yield: 98%. ^{1}H NMR (300 MHz, $CDCl_3$) δ: 2.18 (s, 3H), 7.15−7.18 (m, 1H), 7.26−7.30 (m, 2H), 7.39−7.48 (m, 1H), 7.53−7.55 (m, 2H), 7.63−7.68 (m, 1H), 8.19−8.22 (m, 2H). IR cm^{-1} (KBr): 1733, 1268, 1244.

3-(Bromomethyl)phenyl Benzoate (17). The intermediate **16** (1.3 g, 6.0 mmol), *N*-bromosuccinimide (1.3 g, 7.2 mmol), and 2,2′-azobis(2-methylpropionitrile) were dissolved in 6.0 mL of carbon tetrachloride. The solution was refluxed for 1 h, filtered, and added to *n*-hexane to give a precipitate that was filtered and washed with methanol. Yield: 53%. ^{1}H NMR (300 MHz, $CDCl_3$) δ: 4.51 (s, 2H), 7.16−7.18 (m, 1H), 7.25−7.32 (m, 2H), 7.39−7.46 (m, 1H), 7.52−7.55 (m, 2H), 7.63−7.68 (m, 1H), 8.19−8.22 (m, 2H). IR cm^{-1} (KBr): 1728, 1270, 1240.

2-[7-(Hydroxy)-2-oxo-2*H*-chromen-4-yl]acetamide (18). In a glass vessel 0.80 g (3.2 mmol) of **1a** was added to 8.0 mL (16 mmol) of a 2.0 M solution of ammonia in methanol. The ampule was sealed and placed in an oven at 90 °C for 60 h. The solution was evaporated under vacuum, and the solid obtained was crystallized from ethanol. Yield: 50%. ^{1}H NMR (300 MHz, DMSO-d_6) δ: 3.64 (s, 2H), 6.25 (s, 1H), 7.05 (dd, J_1 = 2.4 Hz, J_2 = 8.8 Hz, 1H), 7.08 (d, J = 2.4 Hz, 1H), 7.17 (s, 1H), 7.63 (s, 1H), 7.68 (d, J = 8.7 Hz, 1H), OH not detectable. IR cm^{-1} (KBr): 3447, 3341, 3148, 1712, 1623.

Synthesis of Pyridyl Compounds 19a,b. Amounts of 0.11 g (0.50 mmol) of **18**, 1.5 mmol of 3-(hydroxymethyl)pyridine (0.15 mL, in the case of **19a**) or 4-(hydroxymethyl)pyridine (0.16 g, in the case of **19b**), 0.38 g (1.5 mmol) of 1,1′-(azodicarbonyl)dipiperidine (ADDP), and 0.38 mL (1.5 mmol) of tributylphosphine were dissolved in 5.0 mL of anhydrous THF, and the mixture was stirred at room temperature for 18 h. The obtained precipitate was filtered, washed with chloroform, and then crystallized from ethanol.

2-[2-Oxo-7-(pyridin-3-ylmethoxy)-2*H*-chromen-4-yl]acetamide (19a). Yield: 40%. Mp: 212 °C (dec). ^{1}H NMR (300 MHz, DMSO-d_6) δ: 3.63 (s, 2H), 5.26 (s, 2H), 6.25 (s, 1H), 7.05 (dd, J_1 = 2.5 Hz, J_2 = 8.8 Hz, 1H), 7.11 (d, J = 2.5 Hz, 1H), 7.17 (br s, 1H), 7.40−7.44 (m, 1H), 7.64 (br s, 1H), 7.67 (d, J = 8.8 Hz, 1H), 7.88 (d, J = 8.0 Hz, 1H), 8.54 (d, J = 4.7 Hz, 1H), 8.68 (s, 1H). IR cm^{-1} (KBr): 1714, 1667, 1615. Anal. ($C_{17}H_{14}N_2O_4$) C, H, N.

2-[2-Oxo-7-(pyridin-4-ylmethoxy)-2*H*-chromen-4-yl]acetamide (19b). Yield: 71%. Mp: 193−4 °C. ^{1}H NMR (300 MHz, DMSO-d_6) δ: 3.63 (s, 2H), 5.30 (s, 2H), 6.25 (s, 1H), 7.04−7.07 (m, 2H), 7.16 (br s, 1H), 7.43 (d, J = 5.6 Hz, 2H), 7.63 (br s, 1H), 7.68 (d, J = 9.6 Hz, 1H), 8.57 (d, J = 5.6 Hz, 2H). IR cm^{-1} (KBr): 3319, 1663, 1627. Anal. ($C_{17}H_{14}N_2O_4$) C, H, N.

Synthesis of Esters 20a,b. Amounts of 0.12 g (0.50 mmol) of **1a**, 1.5 mmol of the suitable benzyl alcohol, 0.38 g (1.5 mmol) of ADDP, and 0.39 g (1.5 mmol) of triphenylphosphine were dissolved in 5.0 mL of anhydrous THF, and the mixture was stirred at room temperature for 18 h. The precipitate was filtered off, the solvent evaporated under vacuum and the oily residue purified by flash chromatography (eluent $CHCl_3$).

Ethyl [7-(Benzyl)oxy-2-oxo-2*H*-chromen-4-yl]acetate (20a). Yield: 61%. ^{1}H NMR (300 MHz, DMSO-d_6) δ: 1.16 (t, J = 7.1 Hz, 3H), 3.64 (s, 2H), 4.09 (q, J = 7.1 Hz, 2H), 5.24 (s, 2H), 6.25 (s, 1H), 7.03−7.09 (m, 2H), 7.33−7.46 (m, 5H), 7.68 (d, J = 8.7 Hz, 1H). IR cm^{-1} (KBr): 1732, 1709, 1615.

Ethyl {7-[(3-Chlorobenzyl)oxy]-2-oxo-2*H*-chromen-4-yl}acetate (20b). Yield: 48%. ^{1}H NMR (300 MHz, DMSO-d_6) δ: 1.16 (t, J = 7.1 Hz, 3H), 3.64 (s, 2H), 4.09 (q, J = 7.1 Hz, 2H), 5.24 (s, 2H), 6.25 (s, 1H), 7.03−7.09 (m, 2H), 7.26−7.35 (m, 3H), 7.54 (s, 1H), 7.68 (d, J = 8.7 Hz, 1H). IR cm^{-1} (KBr): 1736, 1712, 1615.

General Procedure for the Synthesis of Amides 21a−g. An amount of 2.0 mmol of a suitable ester **20a**,**b** was placed in a glass vessel together with 20 mmol of the appropriate amine in a 2.0 N THF solution, commercially available or freshly prepared from the parent liquid amine. The vessel was sealed and placed in an oven at 90 °C for 24−60 h, until the starting ester was consumed as indicated by the TLC control. The solvent was then evaporated under vacuum, and the oily residue was purified by column chromatography or crystallized from absolute ethanol.

2-[7-(Benzyloxy)-2-oxo-2*H*-chromen-4-yl]-*N*-methylacetamide (21a). Crystallized from ethanol. Yield: 50%. Mp: 235−6 °C. ^{1}H NMR (300 MHz, DMSO-d_6) δ: 2.57 (d, J = 4.4 Hz, 3H), 3.64 (s, 2H), 5.22 (s, 2H), 6.22 (s, 1H), 7.02 (dd, J_1 = 2.5 Hz, J_2 = 8.8 Hz, 1H), 7.06 (d, J = 2.5 Hz, 1H), 7.30−7.47 (m, 5H), 7.66 (d, J = 8.8 Hz, 1H), 8.07 (br s, 1H). IR cm^{-1} (KBr): 3303, 1716, 1635, 1614. Anal. ($C_{19}H_{17}NO_4$) C, H, N.

2-{7-[(3-Chlorobenzyl)oxy]-2-oxo-2*H*-chromen-4-yl}-*N*-methylacetamide (21b). Purified by column chromatography (eluent: $CHCl_3$/MeOH, 9.5/0.5 v/v). Yield: 50%. Mp: 174−5 °C. ^{1}H NMR (300 MHz, DMSO-d_6) δ: 2.56 (s, 3H), 3.64 (s, 2H), 5.23 (s, 2H), 6.23 (s, 1H), 7.01−7.08 (m, 2H), 7.39−7.42 (m, 3H), 7.53 (s, 1H), 7.67 (d, J = 8.8 Hz, 1H), 8.07 (br s, 1H). IR cm^{-1} (KBr): 3294, 1718, 1640, 1614. Anal. ($C_{19}H_{16}ClNO_4$) C, H, N.

***N*-Butyl-2-{7-[(3-chlorobenzyl)oxy]-2-oxo-2*H*-chromen-4-yl}-acetamide (21c).** Crystallized from ethanol. Yield: 15%. Mp: 112−3 °C. ^{1}H NMR (300 MHz, $CDCl_3$) δ: 0.87 (t, J = 7.2 Hz, 3H), 1.21−1.31 (m, 2H), 1.38−1.50 (m, 2H), 3.23 (q, J = 6.7 Hz, 2H), 3.64 (s, 2H), 5.10 (s, 2H), 5.51 (br s, 1H), 6.23 (s, 1H), 6.87 (d, J = 2.5 Hz, 1H), 6.91 (dd, J_1 = 2.5 Hz, J_2 = 8.8 Hz, 1H), 7.30−7.34 (m, 3H), 7.43 (br s, 1H), 7.60 (d, J = 8.8 Hz, 1H). IR cm^{-1} (KBr): 3287, 1718, 1638, 1613. Anal. ($C_{22}H_{22}ClNO_4$) C, H, N.

***N*-Benzyl-2-{7-[(3-chlorobenzyl)oxy]-2-oxo-2*H*-chromen-4-yl}-acetamide (21d).** Crystallized from ethanol. Yield: 25%. Mp: 170−1 °C. ^{1}H NMR (300 MHz, $CDCl_3$) δ: 3.69 (s, 2H), 4.42 (d, J = 5.8 Hz, 2H), 5.10 (s, 2H), 5.90 (br s, 1H), 6.22 (s, 1H), 6.86 (d, J = 2.5 Hz, 1H), 6.92 (dd, J_1 = 2.5 Hz, J_2 = 8.8 Hz, 1H), 7.15−7.18 (m, 2H), 7.26−7.37 (m, 6H), 7.43 (br s, 1H), 7.60 (d, J = 8.8 Hz, 1H). IR cm^{-1} (KBr): 3280, 1727, 1639, 1619. Anal. ($C_{25}H_{20}ClNO_4$) C, H, N.

2-[7-(Benzyloxy)-2-oxo-2*H*-chromen-4-yl]-*N*,*N*-dimethylacetamide (21e). Crystallized from ethanol. Yield: 55%. Mp: 162−3 °C. ^{1}H NMR (300 MHz, DMSO-d_6) δ: 2.83 (s, 3H), 3.07 (s, 3H), 3.93 (s, 2H), 5.21 (s, 2H), 6.15 (s, 1H), 6.99 (dd, J_1 = 2.5 Hz, J_2 = 8.8 Hz, 1H), 7.06 (d, J = 2.5 Hz, 1H), 7.30−7.47 (m, 5H), 7.55 (d, J = 8.8 Hz, 1H). IR cm^{-1} (KBr): 1724, 1648, 1611. Anal. ($C_{20}H_{19}NO_4$) C, H, N.

2-{7-[(3-Chlorobenzyl)oxy]-2-oxo-2*H*-chromen-4-yl}-*N*,*N*-dimethylacetamide (21f). Purified by column chromatography (eluent: AcOEt). Yield: 62%. Mp: 159−160 °C. ^{1}H NMR (300 MHz, $CDCl_3$) δ: 3.02 (s, 3H), 3.10 (s, 3H), 3.79 (s, 2H), 5.10 (s, 2H), 6.14 (s, 1H), 6.87 (d, J = 2.5 Hz, 1H), 6.92 (dd, J_1 = 2.5 Hz, J_2 = 8.8 Hz, 1H), 7.29−7.34 (m, 3H), 7.43 (br s, 1H), 7.51 (d, J = 8.8 Hz, 1H). IR cm^{-1} (KBr): 1717, 1644, 1617. Anal. ($C_{20}H_{18}ClNO_4$) C, H, N.

***N*-Butyl-2-{7-[(3-chlorobenzyl)oxy]-2-oxo-2*H*-chromen-4-yl}-*N*-methylacetamide (21g).** Purified by column chromatography (eluent: $CHCl_3$/MeOH, 9.7/0.3 v/v). Yield: 25%. ^{1}H NMR (300 MHz, $CDCl_3$) δ: 0.90−1.03 (m, 3H), 1.25−1.67 (m, 4H), 2.98 (s, 3H) 3.06 (s, 3H), 3.32 (t, J = 7.4 Hz, 1H), 3.41 (t, J = 7.4 Hz, 1H) 3.78 (s, 2H), 5.10 (s, 2H), 6.15 (s, 1H), 6.86 (s, 1H), 6.91 (d, J = 8.8 Hz, 1H), 7.26−7.36 (m, 3H), 7.42 (br s, 1H), 7.49 (d, J = 8.8 Hz, 1H). IR cm^{-1} (KBr): 2958, 2872, 1714, 1639, 1609. Anal. ($C_{23}H_{24}ClNO_4$) C, H, N.

General Procedure for the Preparation of Amines 22a,d,h−j and Free Amines of Mesylates 22b,c. The appropriate intermediate **2c−f** (0.17 g, 0.50 mmol) and a 2.0 M solution of *N*-methylamine or *N*,*N*-dimethylamine in THF (5.0 mL, 10 mmol) were stirred at 50 °C under argon for 5 h. The mixture was then cooled to room temperature, and the inorganic precipitate was filtered off. The solvent was then evaporated, and the resulting solid was purified by column chromatography using AcOEt as eluent.

7-(Benzyloxy)-4-[(methylamino)methyl]-2*H*-chromen-2-one (22a). Yield: 44%. ^{1}H NMR (300 MHz, DMSO-d_6) δ: 2.67 (s, 3H), 4.42 (s, 2H), 5.24 (s, 2H), 6.45 (s, 1H), 7.09 (dd, J_1 = 2.2 Hz, J_2 = 8.8 Hz, 1H), 7.13 (d, J = 2.2 Hz, 1H), 7.33−7.47 (m, 5H), 7.76 (d, J = 8.8 Hz, 1H), NH not detectable. IR cm^{-1} (KBr): 1700, 1611. Anal. ($C_{18}H_{17}NO_3$) C, H, N.

7-(1,3-Benzodioxol-5-ylmethoxy)-4-[(methylamino)methyl]-2*H*-chromen-2-one (22d). Yield: 40%. Mp: 168−170 °C. ^{1}H NMR (300 MHz, DMSO-d_6) δ: 2.33 (s, 3H), 3.81 (s, 2H), 5.09 (s, 2H), 6.01 (s, 2H), 6.28 (s, 1H), 6.89−6.99 (m, 3H), 7.02−7.04 (m, 2H), 7.72 (d, J = 8.8 Hz, 1H), NH not detectable. IR cm^{-1} (KBr): 1705, 1614. Anal. ($C_{19}H_{17}NO_5$) C, H, N.

7-(Benzyloxy)-4-[(dimethylamino)methyl]-2*H*-chromen-2-one (22h). Yield: 61%. ^{1}H NMR (300 MHz, $CDCl_3$) δ: 2.34 (s, 6H), 3.54 (s, 2H), 5.13 (s, 2H), 6.32 (s, 1H), 6.88 (d, J = 2.5 Hz, 1H), 6.93 (dd, J_1 = 2.5 Hz, J_2 = 8.8 Hz, 1H), 7.33−7.45 (m, 5H), 7.77 (d, J = 8.8 Hz, 1H). IR (cm^{-1}): 1723, 1611, 1392. Anal. ($C_{19}H_{19}NO_3$) C, H, N.

7-[(3-Chlorobenzyl)oxy]-4-[(dimethylamino)methyl]-2*H*-chromen-2-one (22i). Yield: 71%. Mp: 78−80 °C. ^{1}H NMR (300 MHz, $CDCl_3$) δ: 2.33 (s, 6H), 3.53 (s, 2H), 5.10 (s, 2H), 6.33 (s, 1H), 6.86 (d, J = 2.5 Hz, 1H), 6.92 (dd, J_1 = 2.5 Hz, J_2 = 8.8 Hz, 1H), 7.28−7.34 (m, 3H), 7.43 (s, 1H), 7.78 (d, J = 8.8 Hz, 1H). IR cm^{-1} (KBr): 1708, 1614, 1385. Anal. ($C_{19}H_{18}ClNO_3$) C, H, N.

4-[(Dimethylamino)methyl]-7-[(3-fluorobenzyl)oxy]-2*H*-chromen-2-one (22j). Yield: 74%. Mp: 84−6 °C. ^{1}H NMR (300 MHz, $CDCl_3$) δ: 2.32 (s, 6H), 3.51 (s, 2H), 5.12 (s, 2H), 6.31 (s, 1H), 6.85 (d, J = 2.5 Hz, 1H), 6.91 (dd, J_1 = 2.5 Hz, J_2 = 8.8 Hz, 1H), 7.00−7.06 (m, 1H), 7.13−7.20 (m, 2H), 7.33−7.40 (m, 1H), 7.79 (d, J = 8.8 Hz, 1H). IR cm^{-1} (KBr): 1704, 1615. Anal. ($C_{19}H_{18}FNO_3$) C, H, N.

7-[(3-Chlorobenzyl)oxy]-4-[(methylamino)methyl]-2*H*-chromen-2-one (Free Amine of 22b). Yield: 18%. ^{1}H NMR (300 MHz, $CDCl_3$) δ: 2.54 (s, 3H), 3.90 (s, 2H), 5.10 (s, 2H), 6.38 (s, 1H), 6.86 (d, J = 2.8 Hz, 1H), 6.92 (dd, J_1 = 2.8 Hz, J_2 = 8.8 Hz, 1H), 7.31−7.34 (m, 3H), 7.43 (s, 1H), 7.60 (d, J = 8.8 Hz, 1H), NH not detectable. IR cm^{-1} (KBr): 1710, 1610. Anal. ($C_{18}H_{16}ClNO_3$) C, H, N.

7-[(3-Fluorobenzyl)oxy]-4-[(methylamino)methyl]-2*H*-chromen-2-one (Free Amine of 22c). Yield: 22%. Mp: 115−7 °C. ^{1}H NMR (300 MHz, DMSO-d_6) δ: 2.32 (s, 3H), 3.81 (s, 2H), 5.23 (s, 2H), 6.29 (s, 1H), 7.00 (dd, J_1 = 2.5 Hz, J_2 = 8.8 Hz, 1H), 7.05 (d, J = 2.5 Hz, 1H), 7.12−7.19 (m, 1H), 7.28−7.31 (m, 2H), 7.40−7.47 (m, 1H), 7.73 (d, J = 8.8 Hz, 1H), NH not detectable. IR cm^{-1} (KBr): 1707, 1611. Anal. ($C_{18}H_{16}FNO_3$) C, H, N.

Mesylates **22b**,**c** were prepared from the corresponding free amines following the general procedure reported below.

General Procedure for the Preparation of Methanesulfonate Salts. The suitable 4-aminoalkyl-7-benzyloxycoumarin derivative (1.1 mmol) was dissolved in dry THF (6.0 mL), and methanesulfonic acid (0.080 mL, 1.2 mmol) was slowly added. The resulting white solid was filtered, washed with dry THF, and crystallized from absolute ethanol.

7-[(3-Chlorobenzyl)oxy]-4-[(methylamino)methyl]-2*H*-chromen-2-one Methanesulfonate (22b). Mp: 213−5 °C. ^{1}H NMR (DMSO-d_6) δ: 2.31 (s, 3H), 2.71 (s, 3H), 4.44 (s, 2H), 5.27 (s, 2H), 6.41 (s, 1H), 7.10 (dd, J_1 = 2.5 Hz, J_2 = 8.8 Hz, 1H), 7.14 (d, J = 2.5 Hz, 1H), 7.37−7.44 (m, 3H), 7.54 (s, 1H), 7.77 (d, J = 8.8 Hz, 1H), 9.01 (s, 2H, dis. with D_2O). IR cm^{-1} (KBr): 1716, 1614. Anal. ($C_{19}H_{20}ClNO_6S$) C, H, N.

7-[(3-Fluorobenzyl)oxy]-4-[(methylamino)methyl]-2*H*-chromen-2-one Methanesulfonate (22c). Mp 215−6 °C. ^{1}H NMR (300 MHz, DMSO-d_6) δ: 2.28 (s, 3H), 2.70 (s, 3H), 4.43 (s, 2H), 5.27 (s, 2H), 6.40 (s, 1H), 7.10 (dd, J_1 = 2.5 Hz, J_2 = 8.8 Hz, 1H), 7.15 (d, J = 2.5 Hz, 1H), 7.16 (m, 1H), 7.28−7.31 (m, 2H), 7.41−7.45 (m, 1H), 7.76 (d, J = 8.8 Hz, 1H), 8.96 (s, 2H, dis. with D_2O). IR cm^{-1} (KBr): 1717, 1615. Anal. ($C_{19}H_{20}FNO_6S$) C, H, N.

4-[(Ethylamino)methyl]-7-[(3-fluorobenzyl)oxy]-2*H*-chromen-2-one Methanesulfonate (22e). Intermediate **2e** (0.25 g, 0.80 mmol) and the commercially available 70% solution of ethylamine in water (3.0 mL) were stirred at room temperature under argon for 3 h. The mixture was then poured into ice−water, and a precipitated side product was filtered off. The solvent was evaporated to dryness and the resulting solid was purified by column chromatography using $CHCl_3$/*n*-hexane/AcOEt, 7/2/1 (v/v/v) as eluent, yielding a red oil that was further transformed into the corresponding mesylate salt according to the procedure described above. Yield: 35%. Mp: 242−4 °C. ^{1}H NMR (300 MHz, DMSO-d_6) δ: 1.25 (t, J = 7.2 Hz, 3H), 2.28 (s, 3H), 3.11−3.12 (m, 2H), 4.42−4.46 (m, 2H), 5.27 (s, 2H), 6.45 (s, 1H), 7.11 (dd, J_1 = 2.5 Hz, J_2 = 8.8 Hz, 1H), 7.15 (d, J = 2.5 Hz, 1H), 7.17−7.20 (m, 1H), 7.29−7.32 (m, 2H), 7.41−7.48 (m, 1H), 7.77 (d, J = 8.8 Hz, 1H), 8.88 (s, 2H, dis. with D_2O). IR cm^{-1} (KBr): 1714, 1613. Anal. ($C_{20}H_{22}FNO_6S$) C, H, N.

7-[(3-Fluorobenzyl)oxy]-4-[(isopropylamino)methyl]-2*H*-chromen-2-one Methanesulfonate (22f). Intermediate **2e** (0.25 g, 0.80 mmol) and the commercially available isopropylamine (2.7 mL, 31 mmol) were refluxed for 2 h. The solution was evaporated to dryness and the resulting oil was purified by column chromatography using $CHCl_3$/*n*-hexane/AcOEt 7/2/1 (v/v/v) as eluent, yielding a yellow oil that was further transformed into the corresponding mesylate derivative according to the procedure described above. Yield: 42%. Mp: 196−8 °C. ^{1}H NMR (300 MHz, DMSO-d_6) δ: 1.33 (d, J = 6.5 Hz, 6H), 2.29 (s, 3H), 3.47 (m, 1H), 4.43−4.47 (m, 2H), 5.29 (s, 2H), 6.47 (s, 1H), 7.12 (dd, J_1 = 2.4 Hz, J_2 = 8.9 Hz, 1H), 7.16 (d, J = 2.4 Hz, 1H), 7.21 (m, 1H), 7.30−7.33 (m, 2H), 7.42−7.49 (m, 1H), 7.81 (d, J = 8.9 Hz, 1H), 8.82 (s, 2H, dis. with D_2O). IR cm^{-1} (KBr): 1713, 1612. Anal. ($C_{21}H_{24}FNO_6S$) C, H, N.

Synthesis of Amines 22g and 22k. 7-[(3-Chlorobenzyl)oxy]-4-(chloromethyl)-2*H*-chromen-2-one **2d** (0.40 g, 1.2 mmol), K_2CO_3 (0.17 g, 1.2 mmol), and benzylamine (0.66 mL, 6.0 mmol) or *N*-benzyl-*N*-methylamine (0.15 mL, 1.2 mmol) were stirred in refluxing absolute ethanol (10 mL) for 2−5 h, until the disappearance of the **2d** spot as indicated by the TLC control. The reaction mixture was cooled to room temperature, the inorganic solid residue was filtered off, the solvent was evaporated, and the resulting oil was purified by column chromatography using $CHCl_3$/*n*-hexane/AcOEt 7/2/1 (v/v/v) as eluent, giving a solid, which was crystallized from absolute ethanol yielding a yellow solid.

4-[(Benzylamino)methyl]-7-[(3-chlorobenzyl)oxy]-2*H*-chromen-2-one (22g). Yield: 18%. Mp: 133−5 °C. ^{1}H NMR (300 MHz, $CDCl_3$) δ: 3.93 (s, 2H), 3.94 (s, 2H), 5.09 (s, 2H), 6.49 (s, 1H), 6.87 (dd, J_1 = 2.5 Hz, J_2 = 8.8 Hz, 1H), 6.90 (d, J = 2.5 Hz, 1H), 7.27−7.39 (m, 8H), 7.43 (s, 1H), 7.54 (d, J = 8.8 Hz, 1H), NH not detectable. IR cm^{-1} (KBr): 3298, 1696, 1610. Anal. ($C_{24}H_{20}ClNO_3$) C, H, N.

4-{[Benzyl(methyl)amino]methyl}-7-[(3-chlorobenzyl)oxy]-2*H*-chromen-2-one (22k). Yield: 46%. Mp: 107−8 °C. ^{1}H NMR (300 MHz, DMSO-d_6) δ: 2.13 (s, 3H), 3.58 (s, 2H), 3.67 (s, 2H), 5.23 (s, 2H), 6.35 (s, 1H), 7.02 (dd, J_1 = 1.9 Hz, J_2 = 8.8 Hz, 1H), 7.05 (d, J = 1.9 Hz, 1H), 7.20−7.39 (m, 5H), 7.41−7.44 (m, 3H), 7.53 (s, 1H), 7.85 (d, J = 8.8 Hz, 1H). IR cm^{-1} (KBr): 1708, 1619. Anal. ($C_{25}H_{22}ClNO_3$) C, H, N.

Synthesis of Azides 23a,b. The appropriate chlorides **2c**,**d** (1.7 mmol) and NaN_3 (0.44 g, 6.8 mmol) were refluxed in absolute ethanol (17 mL) for 2 h. The mixture was cooled to room temperature, and the solid residue was filtered off. The solvent was then evaporated and the resulting oil was purified by column chromatography using *n*-hexane/AcOEt, 8/2 (v/v), as eluent, yielding a yellow solid.

4-(Azidomethyl)-7-benzyloxy-2*H*-chromen-2-one (23a). Yield: 45%. ^{1}H NMR (300 MHz, $CDCl_3$) δ: 4.51 (s, 2H), 5.14 (s, 2H), 6.36 (s, 1H), 6.93 (br s, 1H), 6.96−6.97 (br s, 1H), 7.34−7.46 (m, 6H). IR cm^{-1} (KBr): 2116, 1714, 1614.

4-(Azidomethyl)-7-[(3-chlorobenzyl)oxy]-2*H*-chromen-2-one (23b). Yield: 43%. ^{1}H NMR (300 MHz, $CDCl_3$) δ: 4.51 (s, 2H), 5.11 (s, 2H), 6.38 (s, 1H), 6.90 (d, J = 2.5 Hz, 1H), 6.94 (dd, J_1 = 2.5 Hz, J_2 = 8.8 Hz, 1H), 7.30−7.35 (m, 3H), 7.43−7.47 (m, 2H). IR cm^{-1} (KBr): 2108, 1703, 1611.

Synthesis of Primary Amines 24a,b. To a clear solution of $SnCl_2$ dihydrate (0.66 g, 3.5 mmol) in dry methanol (5.0 mL) was added over 1 h the appropriate 4-(azidomethyl)-7-(benzyloxy)-2*H*-chromen-2-one **23a**,**b** (0.40 mmol) in small portions. The mixture was then stirred at room temperature for 3 h. The solvent was then evaporated, the residue was poured into cold water, the pH was made strongly basic with 3 N NaOH, and then the resulting aqueous solution was extracted with AcOEt. The organic layers were collected, washed with brine, dried over Na_2SO_4, and evaporated in vacuum. The resulting solid was further purified by column chromatography using $CHCl_3$/CH_3OH, 9.7/0.3 (v/v), as eluent, yielding the desired primary amines as white solids.

4-(Aminomethyl)-7-(benzyloxy)-2*H*-chromen-2-one (24a). Yield: 36%. Mp: 135−7 °C (dec). ^{1}H NMR (300 MHz, DMSO-d_6) δ: 3.90 (s, 2H), 5.21 (s, 2H), 6.38 (s, 1H), 6.99 (dd, J_1 = 2.5 Hz, J_2 = 8.8 Hz, 1H), 7.07 (d, J = 2.5 Hz, 1H), 7.30−7.47 (m, 5H), 7.67 (d, J = 8.8 Hz, 1H), 2 NHs not detectable. IR cm^{-1} (KBr): 3391, 3320, 1703, 1611. Anal. ($C_{17}H_{15}NO_3$) C, H, N.

4-(Aminomethyl)-7-[(3-chlorobenzyl)oxy]-2*H*-chromen-2-one (24b). Yield: 39%. Mp: 166−7 °C. ^{1}H NMR (300 MHz, DMSO-d_6) δ: 3.90 (s, 2H), 5.23 (s, 2H), 6.39 (s, 1H), 7.00 (dd, J_1 = 2.5 Hz, J_2 = 8.8 Hz, 1H), 7.07 (d, J = 2.5 Hz, 1H), 7.39−7.48 (m, 3H), 7.53 (s, 1H), 7.69 (d, J = 8.8 Hz, 1H), 2 NHs not detectable. IR cm^{-1} (KBr): 3393, 1711, 1612. Anal. ($C_{17}H_{14}ClNO_3$) C, H, N.

Synthesis of Nitriles 25a,b. An amount of 0.38 mmol of **11a** or **11b** and 0.061 mL (0.76 mmol) of anhydrous pyridine were dissolved in 4.0 mL of anhydrous dioxane. The mixture was cooled at 0 °C with an external ice bath, and trifluoroacetic anhydride (0.068 mL, 0.48 mmol) was added dropwise. The clear solution was allowed to reach room temperature and after 10 min was poured into ice. The aqueous solution was extracted with chloroform and the organic phase was dried over anhydrous Na_2SO_4, filtered, and evaporated under vacuum to give a white solid crystallized from ethanol.

(7-Benzyloxy-2-oxo-2*H*-chromen-4-yl)acetonitrile (25a). Yield: 86%. Mp: 178−9 °C. ^{1}H NMR (300 MHz, DMSO-d_6) δ: 4.37 (s, 2H), 5.23 (s, 2H), 6.32 (s, 1H), 7.09 (dd, J_1 = 2.5 Hz, J_2 = 8.8 Hz, 1H), 7.13 (d, J = 2.5 Hz, 1H), 7.30−7.46 (m, 5H), 7.66 (d, J = 8.8 Hz, 1H). IR cm^{-1} (KBr): 2938, 1714, 1612, 1395, 1283. Anal. ($C_{18}H_{13}NO_3$) C, H, N.

{7-[(3-Chlorobenzyl)oxy]-2-oxo-2*H*-chromen-4-yl}acetonitrile (25b). Yield: 97%. Mp: 180−2 °C. ^{1}H NMR (300 MHz,

DMSO-d_6) δ: 4.37 (s, 2H), 5.25 (s, 2H), 6.33 (s, 1H), 7.09 (d, J = 2.5 Hz, 1H), 7.12−7.14 (m, 1H), 7.37−7.44 (m, 3H), 7.54 (s, 1H), 7.67 (d, J = 8.8 Hz, 1H). IR cm^{-1} (KBr): 2936, 1716, 1613, 1396, 1268. Anal. ($C_{18}H_{12}ClNO_3$) C, H, N.

4-(2-Aminoethyl)-7-[(3-chlorobenzyl)oxy]-2*H*-chromen-2-one Hydrochloride (26). Amounts of 0.033 g (0.10 mmol) of **25b** and 0.048 g (0.20 mmol) of $CoCl_2 \cdot H_2O$ were suspended in 2.0 mL of methanol. An amount of 0.038 g (1.0 mmol) of sodium borohydride was added to the suspension, and the reaction mixture was stirred at room temperature for 1 h. Then 1.0 mL of 2.0 N HCl was added and the organic solvent was evaporated under vacuum. The acid solution was cooled at 0 °C, and an amount of 5.0 mL of a solution of ammonia 30% in water was added. The basic solution was extracted with ethyl acetate and the organic phase dried over anhydrous Na_2SO_4, filtered, and evaporated to dryness, yielding a yellow solid which was dissolved in 2.0 mL of chloroform, and 1.0 mL of 3 N HCl was added. A precipitate was obtained and filtered, corresponding to the hydrochloric salt of the desired product. Yield: 20%. Mp: 113 °C (dec), 176−8 °C. ^{1}H NMR (300 MHz, DMSO-d_6) δ: 3.08 (br, 4H), 5.26 (s, 2H), 6.27 (s, 1H), 7.07 (dd, J_1 = 2.4 Hz, J_2 = 8.8 Hz, 1H), 7.11 (d, J = 2.5 Hz, 1H), 7.42−7.44 (m, 3H), 7.54 (s, 1H), 7.78 (d, J = 8.8 Hz, 1H), 7.96 (br s, 3H, dis. with D_2O). IR cm^{-1} (KBr): 3056, 1723, 1615. Anal. ($C_{18}H_{17}Cl_2NO_3$) C, H, N.

7-Hydroxy-4-(2-hydroxyethyl)-2*H*-chromen-2-one (27). An amount of 0.94 g (4.3 mmol) of commercially available 7-hydroxycoumarin-4-acetic acid **5** was dissolved in 25 mL of anhydrous tetrahydrofuran. The mixture was cooled at 0 °C with an external ice bath, and an amount of 13 mL (13 mmol) of a 1.0 M solution of borane in THF was added dropwise. The mixture was allowed to reach room temperature and stirred for 6 h. The mixture was cooled at 0 °C, and an amount of 20 mL of methanol was added. The solvent was evaporated under vacuum and the residue obtained was dissolved in ethyl acetate, washed with water, dried over anhydrous Na_2SO_4, filtered, and evaporated to give a solid that was purified by flash chromatography (eluent $CHCl_3$/MeOH, 9/1 v/v) to give a white solid of satisfactory purity. Yield: 54%. ^{1}H NMR (300 MHz, DMSO-d_6) δ: 2.86 (t, J = 6.3 Hz, 2H), 3.65−3.71 (m, 2H), 4.80 (t, J = 5.2 Hz, 1H), 6.09 (s, 1H), 6.70 (d, J = 2.2 Hz, 1H), 6.78 (dd, J_1 = 2.2 Hz, J_2 = 8.7 Hz, 1H), 7.63 (d, J = 8.7 Hz, 1H), 10.54 (s, 1H). IR cm^{-1} (KBr): 1686, 1611.

Synthesis of Alcohols 28a,b. The intermediate **27** (0.21 g, 1.0 mmol) was dissolved in 10.0 mL of absolute ethanol, and K_2CO_3 (0.14 g, 1.0 mmol) and the corresponding benzyl bromide (2.0 mmol) were added to the solution, and the mixture was refluxed for 45 min. The precipitate was filtered off, and the organic solution was evaporated under vacuum. The oily residue was purified by flash chromatography (eluent $CHCl_3$/MeOH, 9.5/0.5 v/v) to give a white solid.

7-(Benzyloxy)-4-(2-hydroxyethyl)-2*H*-chromen-2-one (28a). Yield: 53%. ^{1}H NMR (300 MHz, DMSO-d_6) δ: 2.89 (t, J = 6.3 Hz, 2H), 3.66−3.72 (m, 2H), 4.80 (t, J = 5.5 Hz, 1H), 5.21 (s, 2H), 6.17 (s, 1H), 7.01 (dd, J_1 = 2.5 Hz, J_2 = 8.8 Hz, 1H), 7.06 (d, J = 2.5 Hz, 1H), 7.30−7.47 (m, 5H), 7.73 (d, J = 8.8 Hz, 1H). IR cm^{-1} (KBr): 1697, 1614.

7-[(3-Chlorobenzyl)oxy]-4-(2-hydroxyethyl)-2*H*-chromen-2-one (28b). Yield: 67%. ^{1}H NMR (300 MHz, DMSO-d_6) δ: 2.89 (t, J = 6.3 Hz, 2H), 3.69 (t, J = 6.3 Hz, 2H), 4.78 (br s, 1H), 5.23 (s, 2H), 6.18 (s, 1H), 7.02 (dd, J_1 = 2.5 Hz, J_2 = 8.6 Hz, 1H), 7.06 (d, J = 2.5 Hz, 1H), 7.41−7.43 (m, 3H), 7.53 (s, 1H), 7.74 (d, J = 8.6 Hz, 1H). IR cm^{-1} (KBr): 3068, 1718, 1610.

Synthesis of Bromides 29a,b. Amounts of 1.0 mmol of **28a** (0.30 g, for **29a**) or **28b** (0.33 g, for **29b**) and 0.73 g (2.2 mmol) of carbon tetrabromide were dissolved in 10 mL of anhydrous dichloromethane. The mixture was cooled at 0 °C with an external ice bath, and triphenylphosphine (0.53 g, 2.0 mmol) dissolved in 2.0 mL of anhydrous dichloromethane, was added dropwise. The mixture was allowed to reach room temperature and stirred for 1 h. The solvent was evaporated under vacuum and the oily residue was purified by flash chromatography (eluent $CHCl_3$/*n*-hexane, 8/2 v/v, for **29a** and $CHCl_3$/*n*-hexane, 7/3 v/v, for **29b**) to give white solids.

7-(Benzyloxy)-4-(2-bromoethyl)-2*H*-chromen-2-one (29a). Yield: 82%. ^{1}H NMR (300 MHz, DMSO-d_6) δ: 3.34 (t, J = 6.8 Hz, 2H), 3.82 (t, J = 6.8 Hz, 2H), 5.21 (s, 2H), 6.27 (s, 1H), 7.02 (dd, J_1 = 2.2 Hz, J_2 = 9.0 Hz, 1H), 7.08 (d, J = 2.2 Hz, 1H), 7.30−7.47 (m, 5H), 7.75 (d, J = 9.0 Hz, 1H). IR cm^{-1} (KBr): 1727, 1609.

4-(2-Bromoethyl)-7-[(3-chlorobenzyl)oxy]-2*H*-chromen-2-one (29b). Yield: 59%. ^{1}H NMR (300 MHz, $CDCl_3$) δ: 3.30 (t, J = 7.2 Hz, 2H), 3.64 (t, J = 7.2 Hz, 2H), 5.11 (s, 2H), 6.20 (s, 1H), 6.89 (d, J = 2.5 Hz, 1H), 6.95 (dd, J_1 = 2.5 Hz, J_2 = 8.8 Hz, 1H), 7.32−7.33 (m, 3H), 7.44 (s, 1H), 7.50 (d, J = 8.8 Hz, 1H). IR cm^{-1} (KBr): 1718, 1610.

Synthesis of Amines 30a,b. An amount of 0.51 mmol of the suitable bromide **29a**,**b** was added to 3.8 mL (7.6 mmol) of a 2.0 M solution of methylamine (for **30a**) or dimethylamine (for **30b**) in THF, followed by anhydrous K_2CO_3 (0.070 g, 0.51 mmol) and KI (0.009 g, 0.051 mmol). The mixture was stirred at 50 °C overnight. The precipitate was filtered off and the solvent was evaporated under vacuum to give an oily residue that was purified by chromatography (eluent $CHCl_3$/MeOH, 9/1 v/v) and crystallized from ethanol.

7-[(3-Chlorobenzyl)oxy]-4-[2-(methylamino)ethyl]-2*H*-chromen-2-one (30a). Yield: 29%. Mp: 72 °C (dec), 137−9 °C. ^{1}H NMR (300 MHz, DMSO-d_6) δ: 2.34 (s, 3H), 2.84−2.92 (m, 4H), 5.24 (s, 2H), 6.19 (s, 1H), 7.04 (dd, J_1 = 2.5 Hz, J_2 = 8.8 Hz, 1H), 7.08 (d, J = 2.5 Hz, 1H), 7.42−7.44 (m, 3H), 7.54 (s, 1H), 7.76 (d, J = 8.8 Hz, 1H), NH not detectable. IR cm^{-1} (KBr): 1719, 1609. Anal. ($C_{19}H_{18}ClNO_3$) C, H, N.

7-(Benzyloxy)-4-[2-(dimethylamino)ethyl]-2*H*-chromen-2-one (30b). Yield: 20%. Mp: 163−4 °C. ^{1}H NMR (300 MHz, DMSO-d_6) δ: 2.84 (s, 6H), 3.17−3.25 (m, 2H), 3.32−3.40 (m, 2H), 5.23 (s, 2H), 6.28 (s, 1H), 7.06 (dd, J_1 = 2.5 Hz, J_2 = 8.8 Hz, 1H), 7.11 (d, J = 2.5 Hz, 1H), 7.31−7.48 (m, 5H), 7.84 (d, J = 8.8 Hz, 1H). IR cm^{-1} (KBr): 1721, 1617. Anal. ($C_{20}H_{21}NO_3$) C, H, N.

pK_a and log *P* Determination of 22b. pK_a and octanol−water partition coefficient of compound **22b** were determined by potentiometric titration using the Sirius GLpKa instrument implemented by the software RefinementPro (Sirius Analitical Ltd., Forest Row, East Sussex, U.K.). For pK_a determination, a 5×10^{-4} M concentration of the sample in a 0.15 M KCl solution was brought to pH 1.8 through the addition of 0.5 M HCl and then titrated up to pH 12.2 with carbonate-free 0.5 M KOH at a temperature of 25 ± 0.5 °C, under a slow argon flow to avoid CO_2 absorption at high pHs. An analogous measurement has been performed in the absence of compound, for the standardization of the instrument (blank curve). Detailed instrumental procedures can be found elsewhere.[86,87]

The curves of sample and blank titrations were elaborated through a computerized mathematical algorithm with the software RefinementPro to get the differential curve of Bjerrum, that shows the number of free protons from the compound dissociation (n) versus pH. These calculations indicate a pK_a of 7.18 ± 0.05, from three independent measurements.

The experimental log P values was determined through a potentiometric titration in a biphasic system constituted by a solution of 0.15 M KCl saturated with 1-octanol.

In a two-phases system, the dissociation of acids or bases is reduced because of the partitioning. This involves a shift of the Bjerrum plot, toward the right for acids and the left for bases. The new value of dissociation constant measured is an apparent pK_a (poKa).

The entity of pK_a shift allows the determination of the experimental value of log P through the following equations. For monoprotic acid, it is

$$P = \frac{10^{\mathrm{poKa} - \mathrm{p}K_a}}{r} - 1$$

For monoprotic basic, it is

$$P = \frac{10^{pK_a - poKa}}{r} - 1$$

The log P value of **22b** coming from these calculations was 2.48 ± 0.03 (from three separated experiments).

Aqueous Solubility Assay. Compound **22b** was dissolved in DMSO at a concentration of 2 and 180 mg/mL. The appropriate solution was added in portions (2 μL at a time) to 1 mL of a 50 mM Tris-HCl, pH 7.4, or of a 50 mM acetate buffer, pH 3.0, solution at room temperature. Typically a total of 10 additions were made so that the final volume of DMSO was well below 5%. The appearance of the precipitate was detected by an absorbance increase due to light scattering by particulate material, in a dedicated diode array UV spectrometer (GE Healthcare, Uppsala, Sweden). Increased UV absorbance was measured in the 600−820 nm range. In its simplest implementation, the precipitation point (i.e., the upper aqueous solubility limit) was calculated from a bilinear curve fit in a plot of the absorbance (y axis) versus μL of DMSO (x axis). The solubility was 52 ± 5 μg /mL and 2.82 ± 0.35 mg/mL at pH 7.4 and pH 3.0, respectively, as the mean ± SEM of three independent assays.

HDM-PAMPA Permeability Assay. Equation 1 below was used to calculate the *effective* permeability coefficient (P_e):

$$P_e = -\frac{2.303 V_D}{A(t-\tau_{LAG})}\left(\frac{V_A}{V_A+V_D}\right)\log\left[1-\left(\frac{V_A+V_D}{V_D(1-R)}\right)\frac{C_A(t)}{C_D(0)}\right] \quad (1)$$

where A the accessible filter area (cm^2) (i.e., filter area multiplied by filter porosity), t is incubation time (s), V_A and V_D are respectively the volumes in the acceptor and the donor wells (cm^3), $C_A(t)$ is the concentration of the compound (mol cm^{-3}) in the acceptor well at time t, and $C_D(0)$ is the concentration of the compound (mol cm^{-3}) in the donor well at time 0. R is the retention factor, calculated by eq 2 and defined as the mole fraction that is lost in the membrane and in the microplates (i.e., filters and plate materials):

$$R = 1 - \frac{C_D(t)}{C_D(0)} - \left(\frac{V_A}{V_D}\right)\left(\frac{C_A(t)}{C_D(0)}\right) \quad (2)$$

τ_{LAG} is the steady-state time (s), i.e., the time needed for the permeant's concentration gradient to become stabilized. Mathematically τ_{LAG} is the time at which Fick's second law has transformed into the limiting situation of Fick's first law. Steady-state times (τ_{LAG}) to saturate the membranes in PAMPA are short relative to the total permeation time (~20 min with unstirred plates), and for this reason they are usually neglected.

Permeation experiments were carried out in polycarbonate (PC) 96-well microtiter filter plates (Millipore, Bellerica, MA). Filter specifications of PC filter plates were 3 μm pore size, 10 μm thickness, and 12.5% porosity (the manufacturer specifications were 5−20% porosity range; thus, the average porosity value was taken in this work). Each well was coated with 0.75 μL of hexadecane. Because of the high viscosity of hexadecane (HDC), hexane was used as a solvent (15 μL of 5% (v/v) HDC in hexane was dispensed in each well), and after the application of the membrane, the resulting filter plates were placed under a hood for 20 min to completely evaporate the hexane. Subsequently, the donor plate was placed upon a Teflon acceptor plate (MSSACCEPTOR, Millipore, Bellerica, MA) which had been prefilled with 280 μL of buffer containing 5% DMSO. The system was finally hydrated with 280 μL of tested compounds in buffer containing 5% DMSO, and the resulting sandwich was incubated for 5 h at room temperature under constant shaking (75 rpm). Reference compound concentrations were chosen according to their solubility (i.e., 2.5 mM for **22b** and 617 μM for **3**). Each compound was measured in quadruplicate, and iso-pH conditions were used (same pH in donor and acceptor compartments; 0.1 M phosphate buffer solution (pH 6.8) was used).

After 5 h, the sandwich was disassembled and both donor and acceptor compartments were transferred to a UV quartz plate (Hellma GmbH & Co., Mullheim, Germany). UV absorption was measured with a PowerWave (Bio-Tek Instruments, Inc., Winooski, VT), and the reading was performed at λ_{max} of the compounds.

The very low concentration (in both donor and acceptor compartments) of **3** renders the UV detection ineffective, and therefore, the detection was performed using HPLC Merck Hitachi apparatus with a Discovery RP amide C16 (20 mm × 4 mm i.d., 5 μm) (Supelco, Bellefonte, PA).

To assess membrane stability, electrical resistance measurements were conducted on the filter plate at the end of the incubation time, using an electrometer system especially designed for PAMPA assays (EVOMX and MULTI96, World Precision Instruments, Sarasota, FL).

Molecular Modeling. Molecular Building and Optimization. The coumarin inhibitors were built from the Sybyl (version 8.2) fragment libraries starting from the reference ligand (4-FCBC) cocrystallized with hMAO-B (PDB code 2v60). Geometrical optimization and charge calculation were made by means of a quantum mechanical method with the PM3 Hamiltonian. The starting conformation for docking of the 7-(*m*-halogeno)-benzyloxy substituents was recovered from the X-ray crystallographic structures of 4-FCBC and safinamide bound to hMAO-B.[56]

Homology Modeling. The 3D model of the rMAO-B (entry name of AOFB_RAT; primary accession number of P19643 at the ExPASy proteomics server) was developed starting from the X-ray structure of the hMAO-B (PDB code 2v60) complexed with the 4-FCBC ligand. The two MAO-B from different species presented highly close amino acid sequences (520aa vs 520aa, 88% of sequence similarity) and almost identical amino acid residues in the binding site where the only difference was the substitution of Ile316 in human by Val316 in rat. The three-dimensional model of rMAO-B was constructed through homology modeling within Modeller (version 9.2). Among the five best solutions derived from Modeller, the one provided with the lowest value of the Modeller objective scoring function was selected for the subsequent docking simulations. The stereochemical quality of this model, as well as the overall residue-by-residue geometry, was controlled with Procheck (version 3.5.4). By selection of a resolution value equal to 2.0 Å, the Ramachandran plot returned 99.5% of residues in the core regions that represent the most favorable and allowed combinations of φ and ψ angle values while only the remaining 0.5% of residues (Lys52 and Ala346) was located in disallowed regions. As expected, the fitting of the backbone α-carbons of theoretical (rMAO-B) and experimental (hMAO-B) models gave a very low deviation (rms 0.096 Å), indicating a substantial conservation of their spatial position. By Modeller modeling of all the heteroatoms, it was possible to rebuild the coordinates of FAD cofactor and the eight structural water molecules coming from hMAO-B 2v60.

The seven conserved water molecules in hMAO-A crystal structure (PDB code 2z5x) were transferred into the binding site of rMAO-A by using Sybyl.

Docking Simulations. GOLD (version 2.4), a genetic algorithm-based software, was used for a docking study selecting GoldScore as a fitness function. GoldScore is made up of four components that account for protein−ligand binding energy: protein−ligand hydrogen bond energy (external H-bond), protein−ligand van der Waals energy (external vdw), ligand internal vdw energy (internal vdw), and ligand torsional strain energy (internal torsion). Parameters used in the fitness function (hydrogen bond energies, atom radii and polarizabilities, torsion potentials, hydrogen bond directionalities, and so forth) were taken from the GOLD parameter file.

In the present study, the 3D coordinates of hMAO-B (PDB code 2v60), rat and human MAO-A (PDB codes 1o5w and 2z5x, respectively) were retrieved from the Protein Data Bank. The protein preparation for docking study was performed in Sybyl: the cocrystallized ligands were removed; the correct atom type and the bond orders were assigned to FAD cofactor; by use of the Biopolymer tool, hydrogen atoms were added. The structure model of rMAO-B from Modeller was prepared for docking simulation applying the same protocol described above. For each coumarin inhibitor, 10 conformations were generated in a sphere of a 12 Å radius centered on phenolic oxygen atom of Tyr435 and Tyr444 in rMAO-B and rMAO-A, respectively. In our docking runs, the molecular scaffold of the best ranked solution of the 2v60 reference ligand docked into the rMAO-B was set as physical constraint to favor the occurrence of the known binding mode of coumarin inhibitors.

Biological Assays. In Vitro MAO-A and MAO-B Inhibition. MAO Enzyme Source and Membrane Preparations (Crude Rat Brain Mitochondrial Fraction). Male Wistar rats (Harlan, Italy, 150−175 g) were sacrificed under light anesthesia, and brains were rapidly removed and homogenized in 10 volumes of ice-cold 0.32 M sucrose buffer containing 0.1 M EDTA, pH 7.40. The crude homogenate was centrifuged at 2220 rpm for 10 min and the supernatant recovered. The pellet was homogenized and centrifuged again, and the two supernatants were pooled and centrifuged at 9250 rpm for 10 min at 4 °C. The pellet was resuspended in fresh buffer and centrifuged at 11250 rpm for 10 min at 4 °C. The resulting pellet was stored at −80 °C until use.

Human Platelet Rich Plasma (PRP) Preparation. The human venous blood (3.8% sodium citrate as anticoagulant) was immediately centrifuged at 125*g* for 15 min at 4 °C. The supernatant was removed and stored in ice. The pellet was again centrifuged at 600*g* for 5 min at 4 °C. The two PRP supernatants were pooled and stored at −80 °C until assay.

In Vitro MAO-A and MAO-B Inhibition Assays in Rat Brain Mitochondria. The enzyme activities were assessed with a radioenzymatic assay using the selective substrates ^{14}C-serotonin (5-HT) and ^{14}C-phenylethylamine (PEA) for MAO-A and MAO-B, respectively. The mitochondrial pellet (500 μg protein) was resuspended in 0.1 M phosphate buffer, pH 7.40, and 500 μL was added to 50 μL of the test compound or buffer for 30 min at 37 °C (preincubation). Then the substrate (50 μL) was added. The incubation was carried out for 30 min at 37 °C ([^{14}C]5-HT, 5 μM) or for 10 min at 37 °C ([^{14}C]PEA, 0.5 μM). The reaction was stopped by adding 0.2 mL of 37% HCl or 0.2 M perchloric acid. After centrifugation, the deaminated metabolites were extracted with 3 mL of diethyl ether (5-HT) or toluene (PEA) and the radioactive organic phase was measured by liquid scintillation spectrometry at 90% efficiency. Radioactivity in the eluate indicates the production of neutral and acidic metabolites formed as a result of MAO activity. The enzymatic activity was expressed as nanomoles of substrate transformed per milligram of protein per minute. The activity of MAO in the sample was expressed as a percentage of control activity in the absence of inhibitors after subtraction of appropriate blank values.

In Vitro MAO-B Inhibition Assay in PRP Preparation. MAO-B enzyme activity was assessed with a radioenzymatic assay using [^{14}C]PEA as selective substrates (3). The PRP was diluted 1:5 in 0.1 M phosphate buffer, pH 7.40, and 500 μL (in duplicate) was added to 50 μL of buffer and to 50 μL of substrate ([^{14}C]PEA, 0.5 μM). The incubation was carried out for 10 min at 37 °C. The reaction was stopped by adding 0.2 mL of perchloric acid. After centrifugation, the acidic metabolites were extracted by 3.5 mL of toluene and an amount of 3 mL of the radioactive organic phase was added to 10 mL of scintillation cocktail Insta-Fluor and measured by liquid scintillation spectrometry at 90% efficiency.

In Vitro MAO-B Inhibition Reversibility Studies. The reversibility of MAO-B inhibition was assessed performing time-dependent experiments. Time-dependent inhibition kinetics were measured as IC_{50} values after 0 or 30 min of enzyme−inhibitor preincubation. The absence of a significant difference between IC_{50} with or without preincubation was considered as indicative of reversible inhibition.

Ex Vivo MAO-A and MAO-B Inhibition. C57Bl mice were treated with the test compound at different concentrations (0.5 to 20 mg/kg po and ip), and at different time intervals (0.5, 1, 2, 4, 8, 16, and 24 h) they were sacrificed. The brains were removed, and crude homogenates were prepared in 0.1 M phosphate buffer pH 7.40. The enzyme inhibition were performed with a radioenzymatic assay as described above.

In Vitro Human Recombinant Cytocrome P450 Isoform Assay. Inhibition of the six most important P450 isoforms (CYP1A2, CYP2C9, CYP2C19, CYP2D6, CYP2E1, and CYP3A4) was measured in specific assays using suitable substrates that become fluorescent upon CYP metabolism (Gentest Kit assay, BD Biosciences, Bedford, MA). Compounds were tested in a 96-well plate containing incubation/NADPH regenerating buffer. Specific human recombinant isoenzymes (supersomes) and substrates were added and incubated at 37 °C. The specific substrates were the following: 3-cyano-7-ethoxycoumarin (CYP2C19 and CYP1A2), 7-methoxy-4-trifluoromethylcoumarin (CYP2C9), 3-[2-(*N,N*-diethyl-*N*-methylamonium)ethyl]-7-methoxy-4-methylcoumarin (CYP2D6), 7,8-benzoquinoline (CYP3A4), 7-methoxy-4-phenylcoumarin (2E1). The plates were read on a Victo3vr plate reader (Perkin-Elmer, Wellesley, MA) at the appropriate emission/excitation wavelengths. Known inhibitors from literature for each isoenzyme were tested in every assay as positive control.

In Vitro Cell Viability Assay. The SHSY-5Y continuous cell line from a human neuroblastoma (Istituto Zooprofilattico, Brescia, Italy) was chosen from the present study. Cells, showing a neuronal-like morphology and a growth adherent to the plastic culture surface, were routinely maintained in Dulbecco's modified essential medium (DMEM) supplemented with 10% of heat inactivated FBS plus 1% nonessential amino acid, 2 mM glutamine, and 100 U/mL penicillin + 100 μg/mL streptomycin and were grown at 37 °C in an atmosphere of 95% air and 5% CO_2. Culture medium was replaced every 24 h. Growth constituents unless otherwise stated were purchased from Life Technologies. Cells, routinely split 1:5, were transplanted by trypsin−EDTA solution (0.05−0.02% in PBS) and plated according to experimental needing.

The experimental protocol assay was as follows: at time 0 cells were seeded at 6.25×10^4/cm^2 in 96-well cell culture plates in complete growth medium, and after 72 h at subconfluent phase, growth medium was removed and neurobasal medium (with 2 mM glutamine and 100 U/mL penicillin + 100 μg/mL streptomycin, without serum) was added 30 min before the addition of compound **22b**. The assay proceeded with a 24 h incubation at 37 °C in serumless neurobasal medium (200 μL/well) with or without **22b** at 1, 3, 10, 30, and 100 μM. At the end of incubation, cell viability was assessed by a colorimetric assay by using the MTS ([3-(4,5-dimethylthiazol-2-yl)-5-(3-carboxymethoxyphenyl)-2-(4-sulfophenyl)-2*H*-tetrazolium, inner salt]) kit by Promega (Promega Corp., Madison, WI).

Data Elaboration and Statistical Analysis. Enzyme inhibition curves were obtained from at least seven different concentrations, each in duplicate (from 10^{-10} to 10^{-4} M), and the IC_{50} values with confidence intervals were determined using nonlinear regression analysis (GraphPad Prism). Data were expressed as the mean ± SEM and were analyzed by ANOVA followed by Dunnett's test. Generally, SEM values were lower than 15% of the calculated mean.

Acknowledgment. We thank Dr. Sophie Martel and Prof. Pierre-Alain Carrupt from the School of Pharmaceutical Sciences, University of Geneva—University of Lausanne,

Switzerland, for helpful advice on the HDM-PAMPA assay and Dr. Piero Melloni from Newron Pharmaceuticals, Bresso, Italy, for helpful discussions and support in the execution of the present work. The experimental determinations of pK_a and log *P* by Filomena Fiorella, Dipartimento Farmacochimico, University of Bari, Italy, and of the aqueous solubility by Jose Manuel Brea Floriani, Department of Pharmacology, University of Santiago de Compostela, Spain, are kindly acknowledged. The Spanish authors thank the Ministerio de Ciencia e Innovación and the European Regional Development Fund (Madrid, Spain, Grant SAF2007-66114) for financial support.

References

(1) Strolin-Benedetti, M.; Tipton, K. F.; Whomsley, R. Amine Oxidases and Monooxygenases in the in Vivo Metabolism of Xenobiotic Amines in Humans: Has the Involvement of Amine Oxidases Been Neglected? *Fundam. Clin. Pharmacol.* **2007**, *21*, 467–479.
(2) Shih, J. C.; Chen, K.; Ridd, M. J. Monoamine Oxidase: From Genes to Behaviour. *Annu. Rev. Neurosci.* **1999**, *22*, 197–217.
(3) Edmondson, D. E.; Mattevi, A.; Binda, C.; Li, M.; Hubalek, F. Structure and Mechanism of Monoamine Oxidases. *Curr. Med. Chem.* **2004**, *11*, 1983–1993.
(4) Edmondson, D. E.; Binda, C.; Wang, J.; Upadhyay, A. K.; Mattevi, A. Molecular and Mechanistic Properties of the Membrane-Bound Mitochondrial Monoamine Oxidases. *Biochemistry* **2009**, *26*, 4220–4230.
(5) Binda, C.; Newton-Vinson, P.; Hubalek, F.; Edmondson, D. E.; Mattevi, A. Structure of Human Monoamine Oxidase B, a Drug Target for a Treatment of Neurological Disorders. *Nat. Struct. Biol.* **2002**, *9*, 22–26.
(6) Binda, C.; Li, M.; Hubalek, F.; Restelli, N.; Edmondson, D. E.; Mattevi, A. Insights into the Mode of Inhibition of Human Mitochondrial Monoamine Oxidase B from High-Resolution Crystal Structures. *Proc. Natl. Acad. Sci. U.S.A.* **2003**, *100*, 9750–9755.
(7) De Colibus, L.; Li, M.; Binda, C.; Lustig, A.; Edmondson, D. E.; Mattevi, A. Three-Dimensional Structure of Human Monoamine Oxidase A (MAO A): Relation to the Structures of Rat MAO A and Human MAO B. *Proc. Natl. Acad. Sci. U.S.A.* **2005**, *102*, 12684–12689.
(8) Ma, J.; Yoshimura, M.; Yamashita, E.; Nakagawa, A.; Ito, A.; Tsukihara, T. Structure of Rat Monoamine Oxidase A and Its Specific Recognitions for Substrates and Inhibitors. *J. Mol. Biol.* **2004**, *338*, 103–114.
(9) Grimsby, J.; lan, N. C.; Neve, R.; Chen, K.; Shih, J. C. Tissue Distribution of Human Monoamine Oxidase-A and Oxidase-B Messenger-RNA. *J. Neurochem.* **1990**, *55*, 1166–1169.
(10) Fowler, C. J.; Ross, S. B. Selective Inhibitors of Monoamine Oxidase A and B: Biochemical, Pharmacological, and Clinical Properties. *Med. Res. Rev.* **1984**, *4*, 323–358.
(11) Youdim, M. B.; Bakhle, Y. S. Monoamine Oxidase: Isoforms and Inhibitors in Parkinson's Disease and Depressive Illness. *Br. J. Pharmacol.* **2006**, *147*, S287–S296.
(12) Yamada, M.; Yasuhara, H. Clinical Pharmacology of MAO Inhibitors: Safety and Future. *Neurotoxicology* **2004**, *25*, 215–221.
(13) Lewitt, P. A. MAO-B Inhibitor Know-How: Back to the Pharm. *Neurology* **2009**, *72*, 1352–1357.
(14) Youdim, M. B.; Edmondson, D. E.; Tipton, K. F. The Therapeutic Potential of Monoamine Oxidase Inhibitors. *Nat. Rev. Neurosci.* **2006**, *7*, 295–309.
(15) Haefely, W. E.; Burkard, W. P.; Cesura, A. M.; Kettler, R.; Lorez, H. P.; Martin, J. R.; Richards, J. G.; Scherschlicht, R.; DaPrada, M. Biochemistry and Pharmacology of Moclobemide, a Prototype RIMA. *Psychopharmacology* **1992**, *106*, 6–14.
(16) Fernandez, H. H.; Chen, J. J. Monoamine Oxidase-B Inhibition in the Treatment of Parkinson's Disease. *Pharmacotherapy* **2007**, *27*, S174–S185.
(17) Onofrj, M.; Bonanni, L.; Thomas, A. An Expert Opinion on Safinamide in Parkinson's Disease. *Expert. Opin. Invest. Drugs* **2008**, *17*, 1115–1125.
(18) Chen, J. J.; Swope, D. M.; Dashtipour, K. Comprehensive Review of Rasagiline, a Second-Generation Monoamine Oxidase Inhibitor, for the Treatment of Parkinson's Disease. *Clin. Ther.* **2007**, *29*, 1825–1849.
(19) Olanow, C. W.; Hauser, R. A.; Jankovic, J.; Langston, W.; Lang, A.; Poewe, W.; Tolosa, E.; Stocchi, F.; Melamed, E.; Eyal, E.; Rascol, O. A. Randomized, Double-Blind, Placebo-Controlled, Delayed Start Study To Assess Rasagiline as a Disease Modifying Therapy in Parkinson's Disease (the ADAGIO Study): Rationale, Design, and Baseline Characteristics. *Movement Disord.* **2008**, *23*, 2194–2201.
(20) Lee, K. C.; Chen, J. J. Transdermal Selegiline for the Treatment of Major Depressive Disorder. *Neuropsychiatr. Dis. Treat.* **2007**, *3*, 527–537.
(21) Thorpe, L. W.; Westlund, K. N.; Kochensperger, L. M.; Abell, C. W.; Denney, R. M. Immunocytochemical Localization of Monoamine Oxidases A and B in Human Peripheral Tissues and Brain. *J. Histochem. Cytochem.* **1987**, *35*, 23–32.
(22) Strolin Benedetti, M.; Dostert, P. Monoamine Oxidase, Brain Aging and Degenerative Diseases. *Biochem. Pharmacol.* **1989**, *38*, 555–561.
(23) Saura, J.; Andres, N.; Andrade, C.; Ojuel, J.; Eriksson, K.; Mahy, N. Biphasic and Region-Specific MAO-B Response to Aging in Normal Human Brain. *Neurobiol. Aging* **1997**, *18*, 497–507.
(24) Fowler, C. J.; Wiberg, A.; Oreland, L.; Marcusson, J.; Winblad, B. The Effect of Age on the Activity and Molecular Properties of Human Brain Monoamine Oxidase. *J. Neural Transm.* **1980**, *49*, 1–20.
(25) Kovacic, P. Oxidative Stress. *Curr. Med. Chem.* **2001**, *8*, 721–863.
(26) Barnham, K. J.; Masters, C. L.; Bush, A. I. Neurodegenerative Diseases and Oxidative Stress. *Nat. Rev.* **2004**, *3*, 205–214.
(27) Halliwell, B. Oxidative Stress and Neurodegeneration: Where Are We Now? *J. Neurochem.* **2006**, *97*, 1634–1658.
(28) Hermida-Ameijeiras, A.; Mendez-Alvarez, E.; Sanchez-Iglesias, S.; Sanmartin-Suarez, C.; Soto-Otero, R. Autoxidation and MAO-Mediated Metabolism of Dopamine as a Potential Cause of Oxidative Stress: Role of Ferrous and Ferric Ions. *Neurochem. Int.* **2004**, *45*, 103–116.
(29) Riederer, P.; Danielczyk, W.; Grunblatt, E. Monoamine Oxidase-B Inhibition in Alzheimer's Disease. *Neurotoxicology* **2004**, *25*, 271–277.
(30) Thomas, T. Monoamine Oxidase-B Inhibitors in the Treatment of Alzheimers Disease. *Neurobiol. Aging* **2000**, *21*, 343–348.
(31) Ebadi, M.; Sharma, S.; Shavali, S.; El Refaey, H. Neuroprotective Actions of Selegiline. *J. Neurosci. Res.* **2002**, *67*, 285–289.
(32) Eliash, S.; Dror, V.; Cohen, S.; Rehavi, M. Neuroprotection by Rasagiline in Thiamine Deficient Rats. *Brain Res.* **2009**, *1256*, 138–148.
(33) Sano, M.; Ernesto, C.; Thomas, R. G.; Klauber, M. R.; Schafer, K.; Grundman, M.; Woodbury, P.; Growdon, J.; Cotman, C. W.; Pfeiffer, E.; Schneider, L. S.; Thal, L. J. A Controlled Trial of Selegiline, Alpha-Tocopherol, or Both as Treatment for Alzheimer's Disease. *N. Engl. J. Med.* **1997**, *336*, 1216–1222.
(34) Schneider, L. S.; Olin, J. T.; Pawluczyk, S. A Double-Blind Crossover Pilot Study of l-Deprenyl (Selegiline) Combined with Cholinesterase Inhibitor in Alzheimer's Disease. *Am. J. Psychiatry* **1993**, *150*, 321–323.
(35) Tolbert, S. R.; Fuller, M. A. Selegiline in Treatment of Behavorial and Cognitive Symptoms in Alzheimer's Disease. *Ann. Pharmacother.* **1996**, *30*, 1122–1129.
(36) Binda, C.; Hubalek, F.; Li, M.; Herzig, Y.; Sterling, J.; Edmondson, D. E.; Mattevi, A. Crystal Structures of MAO B in Complex with Four Inhibitors of the *N*-Propargylaminoindan Class. *J. Med. Chem.* **2004**, *47*, 1767–1774.
(37) Son, S. Y.; Ma, J.; Kondou, Y.; Yoshimura, M.; Yamashita, E.; Tsukihara, T. Structure of Human Monoamine Oxidase A at 2.2-Å Resolution: The Control of Opening the Entry for Substrates/Inhibitors. *Proc. Natl. Acad. Sci. U.S.A.* **2008**, *105*, 5739–5744.
(38) Novaroli, L.; Reist, M.; Favre, E.; Carotti, A.; Catto, M.; Carrupt, P. A. Human Recombinant Monoamine Oxidase B as Reliable and Efficient Enzyme Source for Inhibitor Screening. *Bioorg. Med. Chem.* **2005**, *13*, 6212–6217.
(39) Bravo, J. Development and Validation of Target-Based Drug Design Tools: Virtual Screening of Monoamine Oxidase Inhibitors. Ph.D. Thesis, Faculté des Sciences, Université de Genève, Switzerland, April 2009.
(40) Kneubuhler, S.; Carta, V.; Altomare, C.; Carotti, A.; Testa, B. Synthesis and Monoamine Oxidase Inhibitory Activity of 3-Substituted 5*H*-Indeno[1,2-*c*]pyridazines. *Helv. Chim. Acta* **1993**, *76*, 1954–1963.
(41) Kneubuhler, S.; Thull, U.; Altomare, C.; Carta, V.; Gaillard, P.; Carrupt, P.-A.; Carotti, A.; Testa, B. Inhibition of Monoamine Oxidase-B by 5*H*-Indeno[1,2-*c*]pyridazines. Biological Activities, Quantitative Structure−Activity-Relationships (QSARs) and 3D-QSARs. *J. Med. Chem.* **1995**, *38*, 3874–3883.
(42) Altomare, C.; Cellamare, S.; Summo, L.; Catto, M.; Carotti, A.; Thull, U.; Carrupt, P. A.; Testa, B.; Stockli-Evans, H. Inhibition of Monoamine Oxidase-B by Condensed Pyridazines and Pyrimidines; Effects of Lipophilicity and Structure−Activity Relationships. *J. Med. Chem.* **1998**, *41*, 3812–3820.
(43) Thull, U.; Kneubuhler, S.; Gaillard, P.; Carrupt, P.-A.; Testa, B.; Altomare, C.; Carotti, A.; Jenner, P.; McNaught, K. S. P.

Inhibition of Monamine Oxidase by Isoquinoline Derivatives: Qualitative and 3D-Quantitative Structure−Activity Relationships. *Biochem. Pharmacol.* **1995**, *50*, 869–877.
(44) Carotti, A.; Carrieri, A.; Chimichi, S.; Boccalini, M.; Cosimelli, B.; Gnerre, C.; Carotti, A.; Carrupt, P. A.; Testa, B. Natural and Synthetic Geiparvarins Are Strong and Selective MAO-B Inhibitors. Synthesis and SAR Studies. *Bioorg. Med. Chem. Lett.* **2002**, *12*, 3551–3555.
(45) Gnerre, C.; Catto, M.; Leonetti, F.; Weber, P.; Carrupt, P.-A.; Altomare, C.; Carotti, A.; Testa, B. Inhibition of Monoamine Oxidases by Functionalized Coumarin Derivatives: Biological Activities, QSARs, and 3D-QSARs. *J. Med. Chem.* **2000**, *43*, 4747–4758.
(46) Catto, M.; Nicolotti, O.; Leonetti, F.; Carotti, A.; Favia, A. D.; Soto-Otero, R.; Mendez-Alvarez, E.; Carotti, A. Structural Insights into Monoamine Oxidase Inhibitory Potency and Selectivity of 7-Substituted Coumarins from Ligand- and Target-Based Approaches. *J. Med. Chem.* **2006**, *49*, 4912–4925.
(47) Bruhlmann, C.; Ooms, F.; Carrupt, P.-A.; Testa, B.; Catto, M.; Leonetti, F.; Altomare, C.; Carotti, A. Coumarin Derivatives as Dual Inhibitors of Acetylcholinesterase and Monoamine Oxidase. *J. Med. Chem.* **2001**, *44*, 3195–3198.
(48) Carotti, A.; Melloni, P.; Thaler, F.; Caccia, C.; Maestroni, S.; Salvati, P. Substituted Aminoalkyl and Amidoalkyl Benzopyran Derivatives. WO 2006/102958 A1, **2006**.
(49) Rendenbach-Muller, B.; Schlecker, R.; Traut, M.; Weifenbach, H. Synthesis of Coumarins as Subtype-Selective Inhibitors of Monoamine Oxidase. *Bioorg. Med. Chem. Lett.* **1994**, *4*, 1195–1198.
(50) Rendenbach, B.; Weifenbach, H.; Teschendorf, H. J. Arylalkoxycumarine. Verfahren zu Ihre Herstellung und Diese Enthalende Therapeutische Mittel. Patent DE 3834861 A1, **1990** (BASF AG).
(51) Chimenti, F.; Secci, D.; Bolasco, A.; Chimenti, P.; Granese, A.; Befani, O.; Turini, P.; Alcaro, S.; Ortuso, F. Inhibition of Monoamine Oxidases by Coumarin-3-acyl Derivatives: Biological Activity and Computational Study. *Bioorg. Med. Chem. Lett.* **2004**, *14*, 3697–3703.
(52) Chimenti, F.; Secci, D.; Bolasco, A.; Chimenti, P.; Bizzarri, B.; Granese, A.; Carradori, S.; Yáñez, M.; Orallo, F.; Ortuso, F.; Alcaro, S. Synthesis, Molecular Modeling, and Selective Inhibitory Activity against Human Monoamine Oxidases of 3-Carboxamido-7-substituted Coumarins. *J. Med. Chem.* **2009**, *52*, 1935–1942.
(53) Santana, L.; Gonzalez-Diaz, H.; Quezada, E.; Uriarte, E.; Yanez, M.; Vina, D.; Orallo, F. Quantitative Structure−Activity Relationship and Complex Network Approach to Monoamine Oxidase A and B Inhibitors. *J. Med. Chem.* **2008**, *51*, 6740–6751.
(54) Carotti, A. MAOs Long March: From Toxic First-Generation Drugs to Isoform-Selective, Reversible and Multi-Target Inhibitors. Presented at the Meeting of ACS-EFMC, Frontiers in CNS and Oncology Medicinal Chemistry, Siena, Italy, October 7−9, **2007**.
(55) v. Pechmann, H. Novel Synthesis of Coumarins. *Ber. Dtsch. Chem. Ges.* **1884**, *17*, 929–936.
(56) Binda, C.; Wang, J.; Pisani, L.; Caccia, C.; Carotti, A.; Salvati, P.; Edmondson, D. E.; Mattevi, A. Structures of Human Monoamine Oxidase B Complexes with Selective Noncovalent Inhibitors: Safinamide and Coumarin Analogs. *J. Med. Chem.* **2007**, *50*, 5848–5852.
(57) Campos-Toimil, M.; Orallo, F.; Santana, L.; Uriarte, E. Synthesis and Vasorelaxant Activity of New Coumarin and Furocoumarin Derivatives. *Bioorg. Med. Chem. Lett.* **2002**, *12*, 783–786.
(58) Mitsunobu, O. The Use of Diethyl Azodicarboxylate and Triphenylphosphine in Synthesis and Transformation of Natural Products. *Synthesis* **1981**, *1*, 1–29.
(59) Vaultier, M.; Knouzi, N.; Carrie, R. Reductiòn d'Azides en Amines Primaires par une Methode Generale Utilisant la Reaction de Staudinger. *Tetrahedron Lett.* **1983**, *24*, 763–764.
(60) Bartra, M.; Romea, P.; Urpi, F.; Villarasa, J. A Fast Procedure for the Reduction of Azides and Nitro Compounds Based on the Reducing Ability of Sn(SR)3-Species. *Tetrahedron* **1990**, *46*, 587–594.
(61) Campagna, F.; Carotti, A.; Casini, G. A Convenient Synthesis of Nitriles from Primary Amides under Mild Conditions. *Tetrahedron Lett.* **1977**, *21*, 1813–1816.
(62) Martel S.; Gasparik, V.; Carrupt P. A. In Silico Tools and in Vitro HTS Approaches To Determine Lipophilicity during the Drug Discovery Process. In *Hit and Lead Profiling*; Faller, B., Urban, L., Eds.; Wiley-VCH: Weinheim, Germany, 2009.
(63) Lipinski, C. A.; Lombardo, F.; Dominy, B. W.; Feeney, P. J. Experimental and Computational Approaches To Estimate Solubility and Permeability in Drug Discovery and Development Settings. *Adv. Drug Delivery Rev.* **2001**, *46*, 3–26.
(64) Fernández, F.; Caamaño, O.; Nieto, M. I.; López, C.; García-Mera, X.; Stefanachi, A.; Nicolotti, O.; Loza, M. I.; Brea, J.; Esteve, C.; Segarra, V.; Vidal, B.; Carotti, A. 1,3-Dialkyl-8-N-substituted Benzyloxycarbonylamino-9-deazaxanthines as Potent Adenosine Receptor Ligands: Design, Synthesis, Structure−Affinity and Structure−Selectivity Relationships. *Bioorg. Med. Chem.* **2009**, *17*, 3618–3629.
(65) Wohnsland, F.; Faller, B. High-throughput Permeability pH Profile and High-Throughput Alkane/Water log *P* with Artificial Membranes. *J. Med. Chem.* **2001**, *44*, 923–930.
(66) Henchoz, Y.; Bard, B.; Guillarme, D.; Carrupt, P. A.; Veuthey, J. L.; Martel, S. Analytical Tools for Physicochemical Profiling of Drug Candidates To Predict Absorption/Distribution. *Anal. Bioanal. Chem.* **2009**, *394*, 707–729.
(67) Caccia, C.; Maj, R.; Calabresi, M.; Maestroni, S.; Faravelli, L.; Curatolo, L.; Salvati, P.; Fariello, R. G. Safinamide: From Molecular Targets to a New Anti-Parkinson Drug. *Neurology* **2006**, *67*, S18–S23.
(68) Robinson, D. S.; Lovenberg, W.; Keiser, H.; Sjoerdsma, A. Effects of Drugs on Human Blood Platelet and Plasma Amine Oxidase Activity in Vitro and in Vivo. *Biochem. Pharmacol.* **1968**, *17*, 109–119.
(69) Malich, G.; Markovic, B.; Winder, C. The Sensitivity and Specificity of the MTS Tetrazolium Assay for Detecting the in Vitro Toxicity of 20 Chemicals Using Human Cell Lines. *Toxicology* **1997**, *124*, 179–192.
(70) Guba, W.; Roche, O. Computational Filters in Lead Generation: Targeting Drug-like Molecules. In *Chemogenomics in Drug Discovery: A Medicinal Chemistry Perspective*; Kubinyi, H., Folkers, G., Eds.; Wiley-VCH: Weinheim, Germany, 2004; pp 325−340.
(71) Pajouhesh, H.; Lenz, G. R. Medicinal Chemical Properties of Successful Central Nervous System Drugs. *NeuroRx* **2005**, *2*, 541–553.
(72) Carotti, A.; Altomare, C.; Catto, M.; Gnerre, C.; Summo, L.; De Marco, A.; Rose, S.; Jenner, P.; Testa, B. Lipophilicity Plays a Major Role in Modulating the Inhibition of Monoamine Oxidase B by 7-Substituted Coumarins. *Chem. Biodiversity* **2006**, *3*, 134–149.
(73) Amadasi, A.; Surface, J. A.; Spyrakis, F.; Cozzini, P.; Mozzarelli, A.; Kellogg, G. E. Robust Classification of "Relevant" Water Molecules in Putative Protein Binding Sites. *J. Med. Chem.* **2008**, *51*, 1063–1067.
(74) Barillari, C.; Taylor, J.; Viner, R.; Essex, J. W. Classification of Water Molecules in Protein Binding Sites. *J. Am. Chem. Soc.* **2007**, *129*, 2577–2587.
(75) Lu, Y.; Wang, R.; Yang, C. Y.; Wang, S. Analysis of Ligand-Bound Water Molecules in High-Resolution Crystal Structures of Protein−Ligand Complexes. *J. Chem. Inf. Model.* **2007**, *47*, 668–675.
(76) Cavasotto, C. N.; Orry, A. J. W. Ligand Docking and Structure-Based Virtual Screening in Drug Discovery. *Curr. Top. Med. Chem.* **2007**, *7*, 1006–1014.
(77) Roberts, B. C.; Mancera, R. L. Ligand−Protein Docking with Water Molecules. *J. Chem. Inf. Model.* **2008**, *48*, 397–408.
(78) Huang, N.; Shoichet, B. K. Exploiting Ordered Waters in Molecular Docking. *J. Med. Chem.* **2008**, *51*, 4862–4865.
(79) Goodford, P. J. A Computational Procedure for Determining Energetically Favorable Binding Sites on Biologically Important Macromolecules. *J. Med. Chem.* **1985**, *28*, 849–857.
(80) Avdeef, A. *Absorption and Drug Development: Solubility, Permeability, and Charge State*; John Wiley & Sons: Hoboken, NJ, 2003.
(81) Cruciani, G.; Crivori, P.; Carrupt, P. A.; Testa, B. Molecular Fields in Quantitative Structure−Permeation Relationships: The VolSurf Approach. *J. Mol. Struct.: THEOCHEM* **2000**, *503*, 17–30.
(82) Crivori, P.; Cruciani, G.; Carrupt, P. A.; Testa, B. Predicting Blood−Brain Barrier Permeation from Three-Dimensional Molecular Structure. *J. Med. Chem.* **2000**, *43*, 2204–2216.
(83) Baker, M.; Rayens, W. Partial Least Squares for Discrimination. *J. Chemom.* **2003**, *17*, 166–173.
(84) Munoz-Torrero, D. Acetylcholinesterase Inhibitors as Disease-Modifying Therapies for Alzheimer's Disease. *Curr. Med. Chem.* **2008**, *15*, 2433–2455.
(85) Cavalli, A.; Bolognesi, M. L.; Melchiorre, C.; Minarini, A.; Rosini, M.; Recanatini, M. Multi-Target-Directed Ligands To Combat Neurodegenerative Diseases. *J. Med. Chem.* **2008**, *48*, 347–372.
(86) Kramer, S. D.; Gautier, J. C.; Saudemom, P. Considerations on the Potentiometric Log P Determination. *Pharm. Res.* **1998**, *15*, 1310–1313.
(87) Avdeef, A.; Box, K. J.; Comer, J. E.; Gilges, M.; Hadley, M.; Hibbert, C.; Patterson, W.; Tam, K. Y. J. pH-metric log P 11. pK_a determination of water-insoluble drugs in organic solvent−water mixtures. *J. Pharm. Biomed. Anal.* **1999**, *20*, 631–641.